

# **BCL(X)L and BCL2 increase the metabolic fitness of breast cancer cells: a single cell imaging study**

**Federico Lucantoni<sup>1,2,\*</sup>, Manuela Salvucci<sup>1,2</sup>, Heiko Dussmann<sup>1,2</sup>, Andreas U Lindner<sup>1,2</sup>, Diether Lambrechts<sup>3,4</sup>, and Jochen HM Prehn<sup>1,2</sup>.**

<sup>1</sup>Department of Physiology & Medical Physics, Royal College of Surgeons in Ireland, Dublin 2, Ireland.

<sup>2</sup>Centre for System Medicine, Royal College of Surgeons in Ireland, Dublin 2, Ireland.

<sup>3</sup>VIB Centre for Cancer Biology, Leuven, Belgium

<sup>4</sup>Laboratory of Translational Genetics, Department of Human Genetics, KU Leuven, Leuven, Belgium

\*Present address: Departamento de Farmacología, Universitat de València; FISABIO (Fundación para el Fomento de la Investigación Sanitaria y Biomédica de la Comunidad Valenciana), Valencia, Spain.

**Correspondence to:** Professor Jochen H M Prehn, Department of Physiology and Medical Physics, Royal College of Surgeons in Ireland, 123 St. Stephen's Green, Dublin 2, Ireland; E-mail: [jprehn@rcsi.ie](mailto:jprehn@rcsi.ie)

**Running title:** BCL2 proteins regulate bioenergetics

**Manuscript content:** 41 Pages, 8 Figures, 11 Supplementary Figures.

**Keywords:** Single cell imaging, BCL2 proteins, Bioenergetics, Mitochondria, OXPHOS, Breast Cancer

**Acknowledgements:** We thank Dr Claus Reimertz for generating the BCL2 and BCL(X)L overexpressing clones, and Dr Bram Boeckx for RNA sequencing. This research was funded by grants from the Irish Cancer Society Collaborative Cancer Research Centre BREAST-PREDICT (CCRC13GAL) and Science Foundation Ireland and the Health Research Board (13/IA/1881; 16/US/3301) to JHMP. We kindly thank Prof Hiroyuki Noji (Osaka University) and Prof. Hiromi Imamura (Kyoto University) for providing the mito-ATeam and cytosolic ATeam plasmids. We also thank Luise Halang and Aisling O'Brien for technical assistance.

**Authors' Contributions:** Conception and design: FL, HD and JHMP; Acquisition of data: FL, HD, MS, AUL, DL; Writing, review, and/or revision of the manuscript: FL, MS, HD and JHMP; Study supervision: JHMP

**Abbreviations:** BCL2 (B-cell lymphoma), FRET (Förster resonance energy transfer), ATP (adenosine triphosphate), OXPHOS (oxidative phosphorylation), VDAC (voltage-dependent anion channel),  $\Delta\Psi_m$  (mitochondrial membrane potential), ER<sup>+</sup> (estrogen receptor positive), STS (staurosporine), FCCP (Carbonyl cyanide-4-(trifluoromethoxy)phenylhydrazone), CFP (Cyan fluorescent protein), TMRM (tetramethylrhodamine methyl ester), IMM (inner mitochondrial membrane), OMM (outer mitochondrial membrane), SILAC (stable isotope labelling with amino acids in cell culture).

**Conflict of Interests:** All authors declare no conflict of interest.

1 **ABSTRACT**

2 The BCL2 family of proteins regulate apoptosis by controlling mitochondrial outer  
3 membrane permeability. However, effects on mitochondrial structure and bioenergetics have  
4 also been reported. Here we comprehensively characterized the effects of BCL2 and  
5 BCL(X)L on cellular energetics in MCF7 breast cancer cells using time-lapse confocal single  
6 cell imaging and mitochondrial and cytosolic FRET reporters. We found that BCL2 and  
7 BCL(X)L increase the metabolic robustness of MCF7 cells, and that this was associated with  
8 increased mitochondrial NAD(P)H and ATP levels. Experiments with the F<sub>1</sub>F<sub>0</sub> synthase  
9 inhibitor oligomycin demonstrated that BCL2 and in particular BCL(X)L, while not affecting  
10 ATP synthase activity, more efficiently coupled the mitochondrial proton motive force with  
11 ATP production. This metabolic advantage was associated with an increased resistance to  
12 nutrient deprivation and enhanced clonogenic survival in response to metabolic stress, in the  
13 absence of profound effects on cell death. Our data suggest that a primary function of  
14 BCL(X)L and BCL2 overexpression in tumor cells is to increase their resistance to metabolic  
15 stress in the tumor microenvironment, independent of cell death signaling.

## 16 INTRODUCTION

17 BCL2 family members regulate the intrinsic apoptosis pathway by controlling the process of  
18 mitochondrial outer membrane permeabilisation (MOMP) (1). Apart from this function,  
19 BCL2 proteins also regulate mitochondrial fusion and fission (2-5). This process is important  
20 for mitochondrial quality control, but also regulates mitochondrial bioenergetics (6). BCL2  
21 proteins may also control mitochondrial metabolism directly. BCL2 and BAX regulate the  
22 activity of the mitochondrial adenine nucleotide translocator (7). BCL(X)L preserves the  
23 physiological conformation of the voltage-dependent anion channel (VDAC) and promotes  
24 exchange of metabolites (8). In neurons, a pool of BCL(X)L has been found to localise in the  
25 inner mitochondrial membrane (IMM) and to interact with  $F_1F_0$  ATP synthase, increasing its  
26 enzymatic activity and stabilizing mitochondrial membrane potential ( $\Delta\Psi_m$ ) (9, 10). A similar  
27 function was attributed to a truncated form of MCL1 that localizes to the matrix (11).

28 A comprehensive characterization of the effects of BCL2 and BCL(X)L on mitochondrial  
29 bioenergetics at the single cell level and its relation to the process of MOMP has rarely been  
30 performed. It is important to dissect these events at this level, as cell death signalling may  
31 affect metabolism and *vice versa* (12, 13). Effects of BCL2 family proteins on bioenergetics  
32 may be particularly important in cancer cells, which undergo periods of metabolic stress, and  
33 indeed often accumulate extraordinary high levels of BCL2 and BCL(X)L as seen in breast  
34 cancer (14-16). Here, we aimed to comprehensively characterize the effects of BCL2 and  
35 BCL(X)L on cellular energetics in breast cancer cells using time-lapse single cell imaging  
36 and mitochondrial/cytosolic ATP FRET reporters.

## 37 RESULTS

### 38 **Characterisation of BCL2 and BCL(X)L overexpressing ER<sup>+</sup> MCF7 breast cancer cells**

39 We assessed absolute BCL2 protein levels in previously characterised MCF7 cells stably  
40 overexpressing BCL2 or BCL(X)L (17-19), using BCL2 quantitative western blotting (20)

41 (Fig. 1A and B). MCF7-pSFFV (control) cells showed a higher BCL2 concentration over  
42 BCL(X)L and MCL1 (Fig. 1A and B). In MCF7-BCL2 cells, BCL2 was present at a  
43 concentration of 5.59  $\mu$ M, while MCF7-BCL(X)L had levels comparable to MCF7-pSFFV  
44 cells (0.35  $\mu$ M). BCL(X)L reached a concentration of 3.5  $\mu$ M in MCF7-BCL(X)L (Fig. 1B).  
45 MCL1, BAX and BAK levels were similar in the three cell lines (Supplementary Fig. 1A and  
46 B). Thus, high BCL2 or BCL(X)L levels were observed in the respective overexpressing cell  
47 lines, with little compensatory alterations in other BCL2 proteins.

48 Next, we analysed the subcellular localization of BCL2 and BCL(X)L in the respective  
49 overexpressing cells, through immunofluorescence. Both BCL2 and BCL(X)L antibodies co-  
50 localised with MitoTracker Red CMXRos, while no signal was detected in the nucleus (Fig.  
51 1C). BCL(X)L cells displayed slightly different sub-localisation pattern when compared to  
52 BCL2 cells, as previously reported in the same cell lines, by Antonietti *et al* (17, 21).

53 We also tested whether BCL2 and BCL(X)L overexpressing MCF7 possessed enhanced  
54 survival rates following exposure to staurosporine (STS; 2  $\mu$ M) or cisplatin (40  $\mu$ M), through  
55 flow cytometry. MCF7-pSFFV were susceptible to both treatments, while BCL2 and  
56 BCL(X)L overexpressing cell lines were less sensitive (Fig. 1D and E).

### 57 **BCL2 and BCL(X)L expressing cells produce similar amounts of mitochondrial ATP by** 58 **employing less mitochondrial NAD(P)H**

59 We transfected cells with a plasmid encoding a mitochondrial targeted ATP FRET probe  
60 (22), which was multiplexed with the  $\Delta\Psi_m$  sensitive dye TMRM, to measure alterations in  
61 mitochondrial ATP levels simultaneously with  $\Delta\Psi_m$  depolarisation or hyperpolarisation (23,  
62 24). To investigate the effects of BCL2 and BCL(X)L on mitochondrial bioenergetics without  
63 contribution from glycolysis, cells were starved for 3 hours and then fuelled with the  
64 mitochondrial substrate pyruvate. Cells were imaged with a laser scanning confocal  
65 microscope every minute (Supplementary Fig. 2A). Baseline values during starvation were

66 recorded for the first 20 minutes, then 2 mM pyruvate was added and single cell kinetics were  
67 followed for another 20 minutes. Finally, ATP synthase inhibitor oligomycin was used to  
68 block the  $F_0$  subunit of the ATP synthase.

69 Pyruvate addition activated mitochondrial ATP production, observed through an increase in  
70 the normalized FRET/CFP ratio in all three cell lines (Fig. 2A). Following oligomycin,  
71 mitochondrial ATP dropped as a result of ATP synthase inhibition (Fig. 2A).  $\Delta\Psi_m$  increased  
72 during pyruvate exposure due to electron transport chain (ETC) activity and further increased  
73 after oligomycin addition, due to proton motive force not being used for ATP production  
74 (Fig. 2A). We compared the absolute FRET/CFP ratio of the 3 different MCF7 clones, which  
75 is more indicative of actual mitochondrial ATP (Fig. 2B). Baseline and post-pyruvate  
76 addition mitochondrial ATP levels were lower in BCL2 cells when compared to MCF7-  
77 pSFFV and BCL(X)L cells. Following oligomycin, ATP levels were similar in all cell lines  
78 (Fig. 2B). Interestingly, a lower absolute TMRM fluorescence was recorded for BCL2 and  
79 BCL(X)L overexpressing cells at baseline (Fig 2D). Furthermore, BCL(X)L cells showed a  
80 significantly higher  $\Delta\Psi_m$  following oligomycin addition, when compared to the other cells  
81 (Fig 2A and C).

82 Using similar treatment protocol, we next measured NAD(P)H kinetics (Supplementary Fig.  
83 2B). An increase in NAD(P)H fluorescence was measured when pyruvate was added to the  
84 experimental buffer (Fig. 2E). Quantification of NAD(P)H levels in the different cells  
85 revealed that during starvation and after pyruvate addition, BCL2 and BCL(X)L cells  
86 accumulated higher NAD(P)H levels (Fig. 2F). Despite lower NAD(P)H levels, MCF7-  
87 pSFFV cells exhibited higher NAD(P)H production kinetics following pyruvate (Fig. 2E).  
88 Slope analyses for pyruvate addition revealed that both MCF7-BCL2 and BCL(X)L  
89 displayed slower NAD(P)H production rates when compared to MCF7-pSFFV (Fig. 2G).  
90 Next, we calculated the NAD(P)H/ATP ratio, by dividing NAD(P)H absolute fluorescence to

91 FRET/CFP absolute ratio. We found that in all conditions MCF7-BCL2 and BCL(X)L cells  
92 accumulated a higher ratio when compared to MCF7-pSFFV cells (Fig. 2H). This suggested  
93 that BCL2 and BCL(X)L overexpressing clones produce similar amount of mitochondrial  
94 ATP, by employing significantly less mitochondrial NAD(P)H.

95 **BCL2 and BCL(X)L overexpressing cell lines couple the mitochondrial proton motive**  
96 **force with ATP production in a more efficient way**

97 We next explored whether BCL2 and BCL(X)L were acting on F<sub>1</sub>F<sub>0</sub> ATP synthase to  
98 enhance mitochondrial energetics of breast cancer cells, by performing an oligomycin  
99 titration. Cells, transiently transfected with mitochondrial ATeam probe, were placed in KB  
100 with 2 mM pyruvate; after 20 minutes of baseline, we applied 1 nM, 10 nM and 100 nM  
101 oligomycin, every 20 minutes (Supplementary Fig. 3). These concentrations were chosen in  
102 order to avoid saturation of ATP synthase. ATP production decreased after addition of 1 nM  
103 of oligomycin in all cell lines, while TMRM signal indicated increased  $\Delta\Psi_m$  (Fig. 3A).  
104 Analysis of FRET/CFP ratios revealed that both MCF7-BCL2 and MCF7-BCL(X)L  
105 possessed higher ATP production following 1 nM oligomycin treatment compared to control  
106 cells. No changes were observed after 10 nM and 100 nM of oligomycin addition, as the  
107 enzyme was likely saturated (Fig. 3B). Of note, an increased TMRM intensity was recorded  
108 in response to oligomycin for MCF7-BCL(X)L cells, compared to control cells (Fig. 3A and  
109 D). Kinetics analysis revealed higher slope values (see Materials and methods, time lapse  
110 imaging section) for BCL2 and BCL(X)L clones after 1 nM oligomycin treatment (Fig. 3C),  
111 indicating slower ATP consumption (since larger negative slope values indicate a faster  
112 descent of the kinetic curve).

113 Next, we determined ATP synthase  $\beta$  subunit protein levels by WB, as it was previously  
114 shown that BCL(X)L can establish an interaction with this subunit (9). As shown in Fig. 3F  
115 no significant difference was detected. We determined the enzymatic activity of

116 immunocaptured ATP synthase from isolated mitochondria by monitoring the oxidation  
117 reaction of NAD(P)H to NAD<sup>+</sup>. Again, no difference was observed (Fig. 3G). Moreover, we  
118 analysed the effect of the proton uncoupler FCCP on cytosolic ATP levels in pyruvate. We  
119 observed that BCL2 and BCL(X)L overexpressing cells maintained higher cytosolic ATP  
120 levels after FCCP treatment (Supplementary Fig. 4). Collectively, these data suggested that  
121 BCL2 and BCL(X)L overexpressing cancer cells possessed higher rates of proton motive  
122 force coupling, with little alterations in ATP synthase activity.

123 **BCL2 and BCL(X)L overexpressing cells maintain higher cytosolic ATP levels during**  
124 **starvation and exhibit higher clonogenic potential during nutrient deprivation**

125 To determine whether these mitochondrial alterations in BCL2 and BCL(X)L cells  
126 precipitated in survival/growth advantage during metabolic stress, we subjected MCF7  
127 clones to nutrient depletion. As starvation has an impact on the cytosolic ATP kinetics, and  
128 we wanted to analyse the ability of BCL2 and BCL(X)L to rescue cell functions by  
129 maintaining cytosolic ATP levels, we here used the cytoplasmic version of the ATeam  
130 construct (22). Cells were placed in KB with no nutrient, and cytosolic ATP levels measured  
131 over 24 hours; (Supplementary Fig. 5A). As shown in Fig. 4A, ATP kinetics decreased  
132 during the time-course. Five mM glucose partially rescued ATP production due to glycolysis  
133 activation (Fig. 4A).  $\Delta\Psi_m$  measured at the same time showed a small initial increase during  
134 the first 2-4 hours, followed by a small decrease (Supplementary Fig. 5B). Measurement of  
135 the FRET/CFP ratio revealed lower baseline values for MCF7-BCL(X)L compared to pSFFV  
136 and BCL2 cells (Fig. 4B). From 12 hours until the end of the experiment, both BCL2 and  
137 BCL(X)L overexpressing cells maintained higher ATP levels compared to control cells (Fig.  
138 4B). Kinetic analysis of ATP consumption highlighted higher slope values for MCF7-BCL2  
139 and BCL(X)L compared to pSFFV cells, from 6 to 20 hours after nutrients removal (Fig. 4C),  
140 suggesting slower ATP loss. TMRM levels were higher for BCL(X)L cells after 2, 6 and 18



141 hours starvation compared to the other cells (Supplementary Fig. 5B).  
142 We next performed clonogenic assay under identical conditions as above. When cells were  
143 cultured in full RPMI medium (NT), BCL(X)L and BCL2 cells revealed a higher capacity to  
144 grow colonies over 7 days compared to MCF7-pSFFV (Fig. 4D and E). Similarly, in the  
145 starvation group [cells placed in SILAC (stable isotope labelling with amino acids in cell  
146 culture) medium with the addition of dialysed fetal bovine serum, without glutamine or  
147 glucose] for 24 hours and then switched to RPMI medium for 7 days, both BCL2 and  
148 BCL(X)L overexpressing cells showed an increased clonogenic potential (Fig. 4D and E).  
149 Similar results were observed when the cells were grown in medium with 5 mM glucose  
150 (SILAC medium without glutamine and supplemented with 5 mM glucose). We also  
151 measured levels of Annexin V/PI negative cells by flow cytometry. A survival of 90 to 100%  
152 was observed in all conditions and cell lines (Fig. 4F). Therefore BCL2 and BCL(X)L  
153 overexpressing cells possessed higher clonogenic potential during metabolic stress, both  
154 during nutrient starvation and in low glucose media, and this effect was not accompanied by  
155 significant cell death induction (Fig. 4E and F).

#### 156 **BCL2 and BCL(X)L cells possess increased mitochondrial respiration during hypoxia**

157 Next, we investigated the potential role for BCL2 proteins in ATP consumption during  
158 hypoxia. First, we employed sodium azide and measured the levels of cytosolic ATP (using  
159 the cytosolic version of the ATeam construct, as we again aimed to analyse the ability of  
160 BCL2 and BCL(X)L to rescue cell functions by maintaining cytosolic ATP levels) when cells  
161 were fuelled with pyruvate (Supplementary Fig. 6). After sodium azide treatment a decrease  
162 in ATP production was observed in all cell lines (Fig 5A), as this prevents cytochrome *c*  
163 oxidase from using O<sub>2</sub>. In parallel, the TMRM fluorescence intensity increased in all cells,  
164 since O<sub>2</sub> is no longer reduced to H<sub>2</sub>O and protons are not pumped to the IMS (Fig. 5A and C).  
165 ATP production was partially restored after glucose addition since glycolysis was activated

166 and compensated for OXPHOS malfunction (Fig. 5A). FRET analysis showed that both  
167 BCL2 and BCL(X)L cells maintained a higher FRET/CFP ratio compared to MCF7-pSFFV  
168 (Fig. 5B). Slope analysis for sodium azide highlighted higher values for BCL2 and BCL(X)L  
169 overexpressing cells compared to control cell line, suggesting a slower ATP consumption  
170 (Fig. 5D).

171 We performed intracellular oxygen measurement using the MitoImage<sup>TM</sup> MM2 probe  
172 (Supplementary Fig. 6B) (25, 26). Cells treated as described in materials and methods, were  
173 placed in KB supplemented with 2 mM pyruvate. After 30 min of baseline recording, oxygen  
174 concentration in the atmosphere was reduced to 2% (Fig 5E). Under 2% O<sub>2</sub>, cells were  
175 treated with 10 μM oligomycin and 5 mM glucose to block ATP synthase related O<sub>2</sub>  
176 consumption. The increase of intracellular O<sub>2</sub> availability recorded was higher in the MCF7-  
177 BCL2 and BCL(X)L (Fig 5E and F). 10 μM FCCP was added to observe maximum  
178 respiration caused by permeabilisation of the inner  $\Delta\Psi_m$  to protons, unrelated to ATP  
179 synthase activity. Finally, O<sub>2</sub> was increased back to ambient concentration showing that 21%  
180 O<sub>2</sub> was saturating the MM2 probe again. We also employed MitoXpress®-Intra (O<sub>2</sub>-sensitive  
181 cell-penetrating nanoparticle probe) to measure intracellular oxygen levels (icO<sub>2</sub>) during  
182 hypoxia (1% O<sub>2</sub> concentration), together with pH (via phenol red absorbance), under the  
183 influence of different substrates. Cells were incubated in SILAC medium plus dialysed FBS  
184 with either 2 mM of glucose, pyruvate or lactate, without glutamine (see Materials and  
185 Methods for details). As shown in Supplementary Fig. 7A we recorded a decrease in icO<sub>2</sub>  
186 after switching to hypoxia. icO<sub>2</sub> reached different plateau among the clones, with BCL(X)L  
187 highlighting higher values in glucose (Supplementary Fig. 7A). We analysed the slope of  
188 oxygen consumption kinetics and found that in glucose, MCF7-BCL(X)L overexpressing  
189 MCF7 possessed slower O<sub>2</sub> consumption rates, when compared to MCF7-pSFFV and BCL2.  
190 Both BCL2 and BCL(X)L cells showed slower consumption kinetics in 2 mM lactate

191 (Supplementary Fig. 7C), while in 2 mM pyruvate, only BCL2 cells showed slower oxygen  
192 consumption when compared to the other clones (Supplementary Fig. 7C). pH  
193 simultaneously decreased with different kinetics from 7.2 to 7.1, in 2 mM lactate or pyruvate  
194 (Supplementary Fig. 7B), while in glucose, pH reached 7.0 in all clones after 10 hours  
195 hypoxia (Supplementary Fig. 7B). We analysed slopes for the pH decrease and found that in  
196 2 mM glucose, MCF7-BCL2 and BCL(X)L overexpressing cells exhibited decreased slope  
197 values compared to MCF7-pSFFV cells, highlighting a faster acidification of the medium  
198 (Supplementary Fig. 7D). On the other hand, in lactate and pyruvate, only MCF7-BCL(X)L,  
199 showed higher pH slope values compared to MCF7-pSFFV and BCL2, highlighting a slower  
200 medium acidification (Supplementary Fig. 7D). We also measured clonogenic potential of  
201 MCF7 clones growth in hypoxia and medium containing 2 mM or 5 mM glucose to simulate  
202 tumour microenvironment (Supplementary Fig. 7E). We observed that MCF7-BCL(X)L cells  
203 grew a higher number of colonies in all conditions, while MCF7-BCL2 showed similar effect  
204 in 5mM glucose, when compared to pSFFV cells (Fig. 5H).

205 **BCL2 and BCL(X)L silencing reduces mitochondrial ATP production following**  
206 **pyruvate addition and reduces clonogenic potential of MCF7 cells**

207 To confirm our results, we employed siRNA to selectively silence BCL2 or BCL(X)L in  
208 MCF7-pSFFV cells. As shown in Supplementary Fig. 8A and B, BCL2 and BCL(X)L protein  
209 levels were reduced by respective siRNAs. Subsequently, we co-transfected the cells with  
210 control (ctrl), BCL2 or BCL(X)L siRNA together with the mitoATeam FRET probe, and  
211 performed the pyruvate experiment of Figure 2 (Supplementary Fig. 9). As shown in Fig. 6A,  
212 we observed an increase in mitochondrial ATP production. However, BCL2 or BCL(X)L  
213 silenced cells registered decreased ATP production kinetics when compared to MCF7-pSFFV  
214 (Fig. 6A). We analysed the absolute FRET/CFP ratio and observed that BCL(X)L siRNA  
215 treated cells possessed lower ATP level, when compared to control siRNA. A trend was seen

216 when comparing BCL2 to control siRNA (Fig. 6B). Of note we found that BCL2 siRNA  
217 treated cells accumulated lower TMRM fluorescence after oligomycin (Fig. 6C) but higher  
218 baseline absolute TMRM (Fig. 6D) when compared to control or BCL(X)L siRNA. To  
219 confirm these results, we repeated similar experiment in the MDA-231 breast cancer cell line,  
220 since these accumulate high levels of BCL2 and BCL(X)L (27). Both BCL2 and BCL(X)L  
221 silenced cells recorded lower mitochondrial ATP levels following pyruvate addition, when  
222 compared to ctrl siRNA transfected cells (Supplementary Fig. 8F). Moreover, we analysed  
223 the clonogenic potential of cells transfected with the different siRNA and found that both  
224 BCL2 and BCL(X)L siRNA treated cells highlighted a lower number of colonies after 7 days  
225 when compared to control siRNA (Fig. 6E and F). No cell death was recorded under same  
226 conditions (Fig. 6G), suggesting a potential block in proliferation upon reduction of BCL2  
227 and BCL(X)L protein levels.

228 **BCL2 and BCL(X)L overexpression improve cell growth and migration in low nutrients**  
229 **conditions**

230 We tested whether overexpression of BCL2 and BCL(X)L could also enhance growth and  
231 migration of breast cancer cells. MCF7 clones were placed in full RPMI or SILAC medium  
232 plus dialysed FBS with 2 mM glucose (without glutamine), and an acid phosphatase assay  
233 used to infer the number of cells. No change in growth was recorded in MCF7 cells placed in  
234 full RPMI (Fig. 7A). However, in 2mM glucose, we found that BCL2 and BCL(X)L  
235 overexpressing cells showed higher number of cells after 4 to 6 days when compared to  
236 MCF7-pSFFV (Fig. 7B). We then performed a wound scratch assay to measure changes in  
237 migration after 24, 48 and 72 hours (Supplementary Fig. 10). We found that both BCL2 and  
238 BCL(X)L overexpressing MCF7 showed a reduced wound area in RPMI, when compared to  
239 control cells (Fig. 7C). Similar results were obtained for cells in 2mM glucose medium at 48  
240 and 72 h timepoints (Fig. 7D), suggesting that BCL2 and BCL(X)L overexpressing cell lines  
241 possess higher proliferation rates and improved migratory capacity during metabolic stress.

## 242 **Gene expression analysis reveals different profiles for respiratory chain complexes**

243 Finally, in order to elucidate potential gene expression changes and mechanisms responsible  
244 for the effects of BCL2 and BCL(X)L in modulating mitochondrial bioenergetics, we  
245 performed RNA-seq experiments of the three MCF7 cell lines. Moreover, we compared these  
246 data with genes expression profiles from publically available breast cancer cell lines and  
247 patient samples. For our in-house dataset, we found that pSFFV and BCL2 clones showed  
248 similar expression patterns. Higher expression in pSFFV and BCL2 overexpressing cell lines  
249 compared to BCL(X)L cells have been found for the majority of respiratory chain complexes.  
250 Nonetheless, COX1, COX2 and COX3 (Complex IV) displayed lowest and highest  
251 expression in BCL(X)L and BCL2 clones, respectively. Additionally, NDUFA11 (Complex  
252 I) expression was lowest in the MCF7-pSFFV cells and increased in the overexpressing  
253 clones. UQCRC1 (Complex II) expression was found altered only in the BCL(X)L  
254 overexpressing cells (Fig. 8). We investigated the association between the expression of  
255 BCL2 and BCL(X)L (BCL2L1) with the expression of the 40 genes found to be statistically  
256 significant different in the analysis of the MCF7 clones in publicly available datasets derived  
257 from cell lines (CCLE, n=50), patient-derived breast cancer xenografts (n=38 PDXs,  
258 Supplementary Figure 11) (28) and tumour resections from the METABRIC (n=1904)  
259 collection. We found that COX1, COX2 and COX3 genes expression is negatively correlated  
260 with BCL2 (small blue dots), consistent with our in house data, showing a lower expression  
261 of these genes in the BCL2 overexpressing clones than in the pSFFV controls. Furthermore,  
262 COX1, COX2, COX3 were found to be positively correlated with BCL(X)L gene expression,  
263 also consistent with findings in our cell lines.

## 264 **DISCUSSION**

265 In this work we described the role of BCL2 and BCL(X)L in regulating breast cancer  
266 bioenergetics. Absolute concentrations of the overexpressed proteins were found to be similar

267 to levels seen in breast cancer patients and other cancer patients (16, 20), or breast tumour  
268 xenografts (29, 30). We found that overexpression of either of these proteins improved ATP  
269 consumption (ability to consume metabolites)/production (efficiency to synthesize ATP) after  
270 various metabolic or toxic challenges.

271 We highlighted that the addition of low pyruvate concentrations increased mitochondrial  
272 ATP synthesis, in line with other studies showing that cancer cells employ OXPHOS (31-33).  
273 Overexpression of BCL2 or BCL(X)L did not increase mitochondrial ATP production after  
274 starvation. Interestingly, after pyruvate addition, NAD(P)H production rates were slower in  
275 BCL2 and BCL(X)L cells when compared to MCF7-pSFFV, suggesting that these cells  
276 produced similar amounts of mitochondrial ATP by consuming/producing less NAD(P)H.  
277 Moreover, BCL2 and BCL(X)L overexpressing cells accumulated higher levels of NAD(P)H,  
278 pointing to an improved bioenergetics status of these cells. Interestingly, we found that levels  
279 of NDUFA11 (Complex I) were higher in overexpressing cell lines.

280 FCCP (and sodium azide), will impair mitochondrial function and elucidate if ATP is still  
281 synthesized under conditions where cells can only employ pyruvate as source of energy, and  
282 glycolysis is not occurring. Oligomycin will specifically and directly impair ATP synthesis  
283 and highlight if ATP synthase is more efficiently working, even when  $\Delta\Psi_m$  is hyper-  
284 polarised. Indeed, these treatments highlighted an increased respiratory capacity of BCL2 and  
285 BCL(X)L overexpressing cells. In fact, FCCP and oligomycin appeared to be more  
286 'effective' in MCF7-pSFFV cells, when compared to cells overexpressing BCL2 and  
287 BCL(X)L, suggesting that both proteins improve coupled respiration and reduce the proton  
288 leak. We also found that BCL(X)L cells accumulated higher  $\Delta\Psi_m$  after oligomycin titration.  
289 This reduced proton leak may be potentially linked to VDAC activity regulation by BCL2  
290 proteins (34, 35), or the ability of BCL2 proteins to form ion channels in lipid bilayers (36).  
291 In our study, we did not observe differences in levels of the ATP synthase subunit  $\beta$ , or in

292 ATP synthase activity between MCF7 control and BCL2 or BCL(X)L overexpressing cells.  
293 A previous study conducted in neurons using patch clamp techniques, showed that BCL(X)L  
294 increased ATP synthase activity through direct binding to the  $\beta$  and  $\alpha$  subunit (9). This could  
295 suggest tissue specific modalities of BCL2 proteins in regulating cell bioenergetics.  
296 Nonetheless, in line with our data, it has been previously shown that BCL(X)L regulates  
297 mitochondrial energetics through the stabilisation of the inner  $\Delta\Psi_m$  in neurons (10). Deletion  
298 or inhibition of BCL(X)L led to large fluctuation of membrane potential by increasing futile  
299 ion flux across the inner mitochondrial membrane, enhancing the probability of an energetic  
300 crisis during stress (10). A different study revealed that recombinant BCL(X)L was able to  
301 restore metabolite exchange across the outer membrane, without inducing the loss of  
302 cytochrome *c* from the intermembrane space through the inhibition of VDAC closure (8).  
303 Together these data suggest that BCL2 proteins improve cellular bioenergetics potentially  
304 through the reduction of the proton leak or through ion exchange through the inner and outer  
305 mitochondrial membrane (8, 37).

306 When cells were starved, both BCL2 and BCL(X)L cells maintained higher ATP  
307 concentration and slower consumption. This was linked to higher NAD(P)H levels as such  
308 levels maintain OXPHOS for longer times (38), and high NAD(P)H autofluorescence is a  
309 marker for increased OXPHOS capacity (39). Cardiac-specific BCL2 overexpression in mice  
310 led to increased NAD(P)H and pyruvate oxidation (40) and reduced the levels of ATP  
311 consumption post-FCCP treatment (41). The slower ATP consumption recorded in  
312 overexpressing cells likely improves their ability to grow under unfavourable conditions.  
313 Indeed, we observed increased clonogenic potential in BCL2 and BCL(X)L cells starved or  
314 grown in reduced glucose. Similar results were observed in normal conditions, suggesting  
315 that BCL2 and BCL(X)L sustained slower ATP consumption/production therefore  
316 consuming less nutrients. This could also explain why we did not observe similar

317 mitochondrial or cytosolic ATP levels, at baseline, across the different clones. Furthermore,  
318 BCL2 and BCL(X)L cells showed increased growth rates and migration in glucose limiting  
319 conditions. The increased nutrient availability might sustain surrounding cell growth  
320 increasing tumorigenic potential of BCL2 and BCL(X)L overexpressing tumours. Moreover,  
321 stabilization of the  $\Delta\Psi_m$  by BCL2 and BCL(X)L might be important for clonogenic growth of  
322 cancer cells, in addition to the observed effects on bioenergetics. Indeed,  $\Delta\Psi_m$  has a role in  
323 the regulation of other processes inside the cells (42-44) and cancer cells usually accumulate  
324 higher  $\Delta\Psi_m$  (45-47).

325 Our results also showed that both BCL2 and BCL(X)L cells maintain higher ATP levels  
326 during chemical hypoxia. Another study linked BCL2 overexpression in human leukaemia  
327 cells to increased oxygen consumption and higher mitochondrial respiration rates (48).  
328 Indeed, our intracellular oxygen imaging approach showed that when ATP synthesis was  
329 blocked, BCL2 and BCL(X)L overexpressing cells showed decreased O<sub>2</sub> consumption,  
330 indicating a close link of O<sub>2</sub> consumption to the activity of the ATP synthase. These effects  
331 could depend on altered levels of cytochrome c oxidase found in our gene expression  
332 analysis. When oxygen concentration was decreased to 1%, under different substrate  
333 availability, BCL2 and BCL(X)L cells registered slower oxygen depletion, indicating a  
334 potential improved adaptation to hypoxia. Indeed, when cells were cultured in glucose  
335 limiting conditions both BCL2 and BCL(X)L cells showed a higher clonogenic potential.

336 In conclusion, we found that BCL2 or BCL(X)L overexpression can increase the resistance of  
337 tumour cells to metabolic stress independent of apoptosis inhibition, by more efficiently  
338 coupling the mitochondrial proton motive force with ATP production. The effects reported in  
339 this manuscript may be important contributors to the oncogenic activity of BCL2 family  
340 proteins and the survival of cancer cells in a metabolically stressed tumour  
341 microenvironment.



342

## 343 **MATERIALS AND METHODS**

### 344 **Materials and reagent**

345 Fetal bovine serum, tetramethylrhodamine methyl ester (TMRM) and Lipofectamine® 2000  
346 were from Invitrogen (Bio Sciences). RPMI 1640 medium, Oligomycin, Carbonyl cyanide 4-  
347 (trifluoromethoxy)phenylhydrazone (FCCP), staurosporine, crystal violet, phenol red, sodium  
348 pyruvate, D-glucose, 2-deoxy-D-glucose, L-glutamine, L-arginine, L-lysine and 4-  
349 Nitrophenyl phosphate disodium salt hexahydrate came from Sigma-Aldrich. Cisplatin  
350 (CDDP) was purchased from Selleckchem. Glass bottom dish (35x10) 12mm aperture used  
351 for time lapse imaging were from WillCo Wells BV. SILAC™ RPMI 1640 Flex Media and  
352 dialysed fetal bovine serum were purchased from Thermo Scientific.

### 353 **Cell lines**

354 MCF7-pSFFV, MCF7-BCL2 and MCF7-BCL(X)L were cultured in RPMI 1640  
355 supplemented with 100 U/mL of penicillin/streptomycin, 10% fetal bovine serum and  
356 incubated at 37°C in humidified atmosphere with 5% of CO<sub>2</sub>. Where specified, MCF7 clones  
357 were placed under SILAC with dialysed FBS, 0.2 g/L arginine, 0.04 g/L lysine and 0.0053  
358 g/L phenol red, without glutamine and with/without the presence of glucose. Cell lines were  
359 free of mycoplasma.

### 360 **Plasmids and transfection**

361 The ATeam1.03-nD/nA/pcDNA3 and MitoATeam1.03 probes (22) were kindly provided by  
362 Prof. Hiroyuki Noji (Osaka University) and Prof. Hiromi Imamura (Kyoto University). Cells  
363 were seeded at a density of  $2 \times 10^3$  onto prewashed, poly-D-lysine (5µg/ml)-coated glass Will-  
364 Co dishes (WillCo Wells BV) and incubated overnight at 37 °C with 5% CO<sub>2</sub>. Twenty-four  
365 hours following seeding, a transfection mix was prepared which consisted of 70 µL of Opti-  
366 MEM, 0.7 µL of Lipofectamine 2000 and 0.2 µg/µL of DNA. After 20 minutes incubation at

367 RT, the medium from each dish was removed, and the transfection mix pipetted onto the  
368 cells. Plates were then incubated for 4 hours at 37 °C. Finally, the media containing this  
369 transfection mix was removed and 2 mL of fresh medium added to each dish.

#### 370 **Generation of cytosolic ATeam stable clones**

371 MCF7-pSFFV, MCF7-BCL2 and MCF7-BCL(X)L were seeded in 6 well plates at a density  
372 of  $1 \times 10^6$  cells per well. Cells were transfected with 200 ng of ATeam plasmid using  
373 Lipofectamine for 4 hours in Opti-MEM medium. After 24 hours transfection was assessed  
374 on a fluorescent microscope and cells cultivated to reach confluency. Subsequently, cells  
375 were trypsinized, diluted 1 in 100 and seeded in new 6 well plates. After 7 days cells were  
376 observed for the presence of fluorescent colonies. Positive cells carrying ATeam plasmid  
377 were then picked up with a p200 pipette, placed in 2 ml medium, gently separated and moved  
378 to a new 6 well plate. The same procedure was then repeated 2-3 times to insure 90-100% of  
379 positive-fluorescent colonies. Cells were then left to reach confluency and moved to a 25  
380 flask and regularly growth.

#### 381 **Western blotting and BCL2 profiling**

382 Cells were scraped, collected and lysed in RIPA buffer (150 mM NaCl, 1.0% IGEPAL® CA-  
383 630, 0.5% sodium deoxycholate, 0.1% SDS, 50 mM Tris, pH 8.0, protease and phosphatase  
384 inhibitors mix 1:100). Protein concentration was determined with micro BCA (bicinchoninic  
385 acid) assay (Pierce, Rockford, IL) and a total of 30 µg of protein loaded into a SDS-gel after  
386 complete denaturation at 90° C for 10 minutes in Laemmli buffer. The samples were then  
387 transferred to nitrocellulose membrane and blocked in TBS-T/5 % milk for 1 h. Primary  
388 antibodies to MCL1 (1:250; BD Biosciences), BCL2 (1:100; Santa Cruz Biotechnology),  
389 BCL(X)L (1:250; Santa Cruz Biotechnology, Inc.), ATP synthase sub.  $\beta$  (1:1000; Invitrogen)  
390 and tubulin (1:5,000; Sigma) were mouse monoclonal. Antibodies to BAK (1:250; Santa  
391 Cruz Biotechnology, Inc.) and BAX (1:1,000; Upstate Biotechnology) were rabbit

392 polyclonal. The horseradish peroxidase (HRP)-conjugated secondary antibodies were from  
393 Jackson ImmunoResearch (1:5000). Detection of protein bands was carried out using  
394 chemiluminescence (EMD Millipore) on a LAS-3000 Imager (FUJIFILM UK Ltd). BCL2  
395 profiling and absolute protein concentration was carried on as previously described (20) and  
396 all densitometry analysis was performed with ImageJ. Briefly, standard calibration curves  
397 were constructed with varying concentrations (0.1–10.0 ng) of recombinant BCL2 proteins  
398 and HeLa extract, by plotting blot intensity against mass of loading. Cellular concentrations  
399 for BCL2 proteins in cellular lysates were calculated from calibration curves, considering  
400 HeLa cell volume of 3.1 pL (20) and the appropriate molecular weights for BAK, BAX,  
401 BCL2, BCL(X)L, and MCL1.

#### 402 **Immunofluorescence of BCL2 and BCL(X)L**

403 MCF7 cell lines were cultured on 13-mm cover slips for 24 hours. On the next day cells were  
404 stained for 30 min at 37° C with MitoTracker Red CMXRos (Thermo Fisher  
405 Scientific) to stain mitochondria, subsequently fixed with 4% paraformaldehyde (PFA,  
406 Affymetrix) for 10 min and permeabilized with 95% ethanol, 5% glacial acetic acid. For  
407 detection of BCL2, a mouse monoclonal anti-BCL2 (clone 8E12, Thermo Fisher Scientific)  
408 and an Alexa Fluor® 488-conjugated secondary anti-mouse (Thermo Fisher Scientific) were  
409 used. For immunostaining of BCL(X)L a rabbit monoclonal anti-BCL(X)L (clone 54H6, Cell  
410 Signaling) and an Alexa Fluor® 488-conjugated secondary anti-rabbit (Thermo Fisher  
411 Scientific) were used. Coverslip were mounted on a microscope slide with ProLong® Gold  
412 Antifade Mountant (Thermo Fisher Scientific) with DAPI to visualize nuclei. Imaging was  
413 performed with a LSM 710 confocal microscope (Carl Zeiss, Germany) using 405, 488, and  
414 561 nm for DAPI, Alexa Fluor 488 and MitoTracker Red laser excitation, respectively, and  
415 using the proper emission bands of the detection unit. Each field of view was acquired with a  
416 stack covering the whole cell body with an optical slice thickness of 1 µm (FWHM) and steps

417 of 0.20 mm with a 100 × 1.4 NA oil immersion plan apochromat objective. Subsequently, the  
418 stacks were de-convolved using Autoquant X (version 2.1.0, Media Cybernetics, UK) and  
419 image further processed with ImageJ 1.45s (National Institutes of Health, Bethesda, MD,  
420 USA).

#### 421 **Flow Cytometry**

422 Cells were treated with 40 μM Cisplatin and 2 μM STS for 24 hours at 37° C. After  
423 incubation time cells were collected by trypsinization and stained with Annexin V-FITC and  
424 propidium iodide (Biovision) for 20 minutes at room temperature in dark condition and  
425 analyzed using a CyFlow ML (Partec) flow cytometer and FloMax software. A minimum of  
426 10,000 events were recorded for each sample. Surviving cells were defined as the fraction of  
427 Annexin V and PI negative cells. The percentage of apoptotic cells was defined as Annexin V  
428 positive/ PI negative plus Annexin V positive/ PI positive.

#### 429 **Clonogenic Assay**

430 MCF7 cell lines were seeded at a density of 1000 cells per well in 6 well plate. Starvation  
431 conditions were mimicked by using SILAC medium (Thermo Scientific) with dialysed FBS  
432 (Thermo Scientific), 0.2 g/L arginine, 0.04 g/L lysine and 0.0053 g/L phenol red (Sigma-  
433 Aldrich). No glucose or glutamine was added to the medium. After 24 hours treatment cells  
434 medium was replaced with fresh RPMI 1640. 5 mM glucose medium were achieved by using  
435 above described SILAC medium with the addition of 5 mM D-glucose. After a week  
436 incubation cells were washed and fixed with 4% PFA (Affymetrix) and stained with 0.5%  
437 crystal violet. Plates were scanned on a CanoScan LiDE 80 (Canon) at a resolution of 1200  
438 ppi. Images were then cropped with ImageJ and analyzed with OpenCFU software (49).

#### 439 **Time lapse imaging**

440 Cells were seeded at a concentration of  $2 \times 10^3$  in sterile Willco dishes and let to adhere over-  
441 night. Then, ATeam constructs were transfected according to the protocol described above.

442 On the day of the experiment, adherent cells were washed twice with krebs-hepes buffer (KB,  
443 140 mM NaCl, 5.9 mM KCl, 1.2 mM MgCl<sub>2</sub>, 15 mM HEPES) and the medium replaced with  
444 1 mL of KB containing 30 nM TMRM, 2 mM sodium pyruvate and 2.5 mM CaCl<sub>2</sub>; an  
445 equilibration time of 40 minutes was applied before starting the imaging procedure. For  
446 experiments in Fig. 2, KB with CaCl<sub>2</sub> without pyruvate was first used for 3 hours, followed  
447 by replacement to KB with TMRM, CaCl<sub>2</sub> and 2mM pyruvate. Mineral oil was added on top  
448 of the KB to prevent evaporation and the dishes transferred to a heated stage (37°C) in a 5%  
449 CO<sub>2</sub> environment above a 63x/1.4 NA Plan-Apochromat oil immersion objective lens on an  
450 inverted confocal laser-scanning microscopes (LSM 710, Carl Zeiss). Mitochondrial ATP  
451 kinetics measurements were carried out using lasers of 405, 488 and 561 nm for excitation of  
452 FRET/CFP, YFP and TMRM respectively with a pixel dwell time of 2.55 μs and images  
453 taken every minute. Detection ranges were set to 445-513 nm and 513-562 nm for CFP and  
454 FRET/YFP, while 562-710 nm was used for TMRM with pinholes set to 2 μm optical  
455 sectioning (FWHM). For NAD(P)H kinetics measurement MCF7 clones were prepared as  
456 before and the medium replaced with 1 mL of KB with 2 mM pyruvate and 2.5 mM CaCl<sub>2</sub>.  
457 Mineral oil was added on top of KB to prevent evaporation and the dishes transferred to a  
458 heated stage (37°C) in a 5% CO<sub>2</sub> environment above a 40x/1.3 Numerical Aperture (NA)  
459 Plan-Neofluar of an inverted epifluorescence microscope (Axiovert 200M, Carl Zeiss).  
460 NAD(P)H was measured through autofluorescence as the reduced form of these molecules is  
461 different from the oxidized form as they absorb and emit light at 340 nm and 445 nm,  
462 respectively. These experiments were carried out using 25% of a HBO 100 mercury short-arc  
463 lamp for excitation with illumination wavelength of 340/20 nm for NAD(P)H excitation with  
464 an exposure time of 100 ms, and a binning of 4x4. Emission was collected at 447/60 nm and  
465 images taken every minute. All kinetics were measured for twenty minutes without treatment  
466 in order to obtain a baseline signal. Images were processed using ImageJ2 (National Institutes

467 of Health, Bethesda, MD, USA) and Metamorph 7.5 (Universal Imaging Co., Westchester,  
468 PA, USA). Time-lapse sequences were imported into ImageJ and background was first  
469 subtracted from each image. After creating combined images of the three fields of views for  
470 each channel sequence, a median filter with a radius of one pixel was applied. The combined  
471 images were then processed using Metamorph. Mitochondria within cells were segmented  
472 from background using the YFP time lapse images. The segmented mitochondrial areas were  
473 converted into a mask used to remove background values from any further analysis of the  
474 FRET/CFP stack. To this end the FRET image stack was first multiplied by the YFP-mask  
475 and divided by CFP image stack, and regions of interest were then selected for analysis.

476 For cytosolic ATP measurement, stable expressing ATeam MCF7 clones were seeded in  
477 sterile Willco dishes. For the FCCP and sodium azide treatment, on the day of the  
478 experiment, KB with 30 nM TMRM, 2 mM sodium pyruvate and 2.5 mM CaCl<sub>2</sub> was added  
479 on top of the cells, with mineral oil to prevent evaporation; an equilibration time of 40  
480 minutes was applied before starting the imaging procedure. For the starvation experiment,  
481 KB with 30 nM TMRM and 2.5 mM CaCl<sub>2</sub> was used instead. The dishes were transferred to a  
482 heated stage (37°C) in a 5% CO<sub>2</sub> environment above a 40×/1.3 Numerical Aperture (NA)  
483 Plan-Neofluar oil immersion objective lenses on an inverted epifluorescence microscope  
484 (Axiovert 200M, Carl Zeiss), used with selected polychroic mirror and filter wheel settings.  
485 Experiments were carried out using 0.09% of a HBO 100 mercury short-arc lamp for  
486 excitation with a band pass of 438/24 nm (center wavelength and band width) for FRET/CFP  
487 (cyan fluorescent protein) and a band pass filter with 500/24 nm YFP (yellow fluorescent  
488 protein) with exposure time of 20 ms. CFP emission was measured in the range of  
489 483/32 nm and FRET/YFP emission in the range of 542/27 nm. TMRM was exposed to  
490 531/40 nm for of 10 ms and detected in the emission range of 593/40 nm (all filters from  
491 Semrock). For all experiments, a custom made Metamorph journal was used to obtain the

492 average intensity signal from all regions, and an excel macro was then applied to sort the  
493 values and to converted them to percentage normalised to the baseline (each cell line was  
494 normalized to its own baseline). All experiments were performed at least three times  
495 independently of each other. For mito ATeam and cytosolic ATeam experiments, slope  
496 values were assessed from normalised traces:  $\Delta$ FRET was calculated by subtracting the  
497 minimal fluorescence value obtained following treatment (offset) to the fluorescence value at  
498 the onset.  $\Delta$ time was calculated accordingly by subtracting the time when the probe reached  
499 the minimal value to the time at the onset. The slope over time was finally obtained by  
500 dividing  $\Delta$ FRET to  $\Delta$ time. For NADH experiment, a non linear fit function  
501 ( $Y = \text{Autofluorescence max} * X / (K_m + X)$ ) in GraphPhad Prism was employed to obtain  $K_m$   
502 values.

### 503 **Mitochondrial isolation and ATP synthase activity assay**

504 ATP synthase activity measurement was carried on with a commercially available kit from  
505 Abcam, following mitochondrial isolation. Mitochondria were isolated accordingly to Frezza  
506 *et al* (50). Briefly, MCF7 clones were seeded in t175 flasks and allowed to reach 80-90%  
507 confluency. Then, cells were detached, collected with fresh medium in 50 mL falcon tubes  
508 and centrifuged at 600 x g for 10 min at 4 °C. The supernatant was discarded and 3 mL of  
509 ice-cold isolation buffer (0.1 M Tris–MOPS, 0.1 M EGTA/Tris, 1 M sucrose and pH at 7.4)  
510 were added. Cells were homogenised using a tissue homogenizer at 708 x g per 6 times, and  
511 centrifuged again at 600 x g for 10 min at 4 °C. Then, the supernatant was collected in a 15  
512 mL falcon tube and centrifuged at 7,000g for 10 min at 4 °C. The supernatant was discarded  
513 and the pellet washed with 200  $\mu$ L of ice cold isolation buffer, resuspended in 200  $\mu$ L and  
514 transferred to a 1.5 mL Eppendorf tube. The homogenate was then centrifuged at 7,000g for  
515 10 min at 4 °C, supernatant discarded and pellet resuspended in 50  $\mu$ L of ice-cold isolation  
516 buffer. The homogenate sample underwent 2 cycles of freeze-thaw, and then centrifuged at

517 16,100 x g for 10 min at 4 °C. The sample was then diluted with 100 µL of solution 1 from  
518 the kit, and the protein concentration assessed with BCA assay. Protein concentration was  
519 adjusted to 5.5 mg/ml and 1/10 volume of detergent solution added. After 30 min incubation  
520 on ice the samples were centrifuged at 16,100 x g for 20 min at 4 °C and the pellet discarded.  
521 The microplate from the kit was then loaded with 50 µL of solution 1, and 2.5 µg of each  
522 sample. Empty wells with the solution 1 alone were added as background control. The  
523 microplate was then stored at 4 °C overnight to let the ATP synthase enzymes bound the  
524 antibody-coated surface of each well. The next day, wells were emptied and washed with 300  
525 µL of solution 1. Subsequently, 40 µL of lipid mix were added to each well and the  
526 microplate incubated at RT for 45 min. After incubation time, 200 µL of reagent mix were  
527 pipetted into each well and the plate inserted into the Clariostar reader at 30 °C. Absorbance  
528 was recorded at 340 nm, with a kinetic program every minute for 2 hours. An excel template  
529 was used to calculate the activity (after background subtraction and according to  
530 manufacturer protocol), and normalized to ATP synthase sub. β levels from Western Blotting  
531 (WB) experiments.

### 532 **Intracellular O<sub>2</sub> and pH measurement using MitoXpress®-Intra**

533 Intracellular oxygen assay was performed using commercially available MitoXpress®-Intra  
534 (NanO<sub>2</sub>) from Luxcel Biosciences (Cork, Ireland). This fluorophore is an O<sub>2</sub>-sensitive cell-  
535 penetrating nanoparticle probe, whose phosphorence is quenched by oxygen such that  
536 measured signal is proportional to intracellular oxygen concentration. MCF7 clones were  
537 seeded at a concentration of  $1.5 \times 10^3$  in a Nunc Micro Well 96 well optical bottom plate. After  
538 overnight incubation, the medium was removed and cells were stained with 100 µL of fresh  
539 medium containing 5 µg/mL of MitoXpress®-Intra and 1 µg/mL Hoechst 33588, for 24  
540 hours. Before the measurements, the staining medium was replaced with SILAC medium  
541 with dialysed FBS, 0.2 g/L arginine, 0.04 g/L lysine, 0.0053 g/L phenol red and 2 mM



542 glucose, pyruvate or lactate as indicated (without glutamine). The plate was placed in a plate  
543 reader at 37 °C, 5% CO<sub>2</sub>, and 21% O<sub>2</sub> (ClarioStar, BMG Labtech, Germany). After 3 hours in  
544 normoxia (21% O<sub>2</sub>), oxygen was decreased to 1% through the plate reader atmospheric  
545 regulator and time-resolved fluorescence measured every 5 minutes for 24 hours. A custom-  
546 made scripting function for the assay was employed. Fluorescent intensities were measured at  
547 delay times of 30 μs and 70 μs, with 30 μs window time, through the bottom optic. The probe  
548 was excited at 340-400 nm and excitation was collected at 635-655 nm, using a bandpass  
549 filter. A gain of 3000 was used for all experiments. To account for changes in proliferation  
550 rates, nuclei were stained with Hoechst and the nanoprobe fluorescence values were  
551 normalized to absolute Hoechst fluorescence. We only considered data from the start of the  
552 experiment until 600 minutes, as no significant change was observed after 10 hours, and to  
553 exclude excessive cell death due to limited nutrient and oxygen availability. Hoechst was  
554 excited 355/20 nm and emission collected at 455/30 nm with a gain at 1500. Values were  
555 analysed with a custom excel template to obtain intracellular oxygen concentration (IcO<sub>2</sub>)  
556 based on the calibration in Fercher *et al* (51) after subtraction of blank (medium without  
557 cells). Then, both IcO<sub>2</sub> and pH signals were divided by the Hoechst signal in order to  
558 accounts for proliferation. pH was recorded in parallel through the measurement of phenol  
559 red absorbance spectra. The wavelength range was 350-650 nm with a step width of 5 nm and  
560 a bidirectional mode was employed for the reading. An excel template was utilised to  
561 calculate the 560/440 nm ratio and the formula  $\log \left[ \frac{560nm}{460nm} \right] / 1.18$  was employed to obtain pH  
562 values. icO<sub>2</sub> slopes were measured using a one phase exponential decay function in GraphPad  
563 Prism, while pH slopes, obtained from measurement of phenol red absorbance spectra, were  
564 measured using a linear regression Line function in the same software.

565 **Monitoring changes in O<sub>2</sub> concentration using the ratiometric MM2 probe**

566 MCF7-pSFFV, MCF7-BCL2 or MCF7-BCL(X)L cells were grown in 4 chamber glass  
567 bottom dishes (CellView, Greiner, Germany). The nanoparticle-based phosphorescent probe,  
568 MitoImage<sup>TM</sup>-MM2, which consists of the O<sub>2</sub>-sensitive phosphorescent reporter dye  
569 (PtTFPP), O<sub>2</sub>- insensitive component (PFO) embedded in a cationic polymer, was purchased  
570 from (Luxcel now Agilent, Ireland) (26, 52). Cells were loaded with 10 µg/ml of MM2 in  
571 RPMI medium supplemented with 1% FBS medium for 16 h at 37°C. MM2 probe intensity  
572 ratio was recorded on an LSM 7live Duoscan confocal microscope (Carl Zeiss, Germany)  
573 equipped with a 40×, 1.3 NA Plan-Neofluar oil-immersion objective and a thermostatically  
574 regulated chamber at 37°C in a humidified atmosphere of 5% CO<sub>2</sub> and the O<sub>2</sub> concentration  
575 as given in the figures (Pecon, Germany). The MM2 probe was excited using 5% of the 30  
576 mW 405 nm DPSS Laser, and the emission was collected through a 415–480 nm band pass  
577 and a 570 nm long pass filter using a 565 nm secondary dichroic to split the emission  
578 between the 2 detectors. Cells were placed in KB with the addition of 2 mM pyruvate. After  
579 baseline measurement, oxygen concentration was reduced to 2%; after 90 minutes 10 µM  
580 Oligomycin and 5 mM glucose were added to stop ATP synthase related O<sub>2</sub> consumption.  
581 Signal was measured for 60 min and 10 µM FCCP added for maximum respiration for 1h; for  
582 the last hour of the experiment O<sub>2</sub> was increased to ambient concentration. All images were  
583 processed using ImageJ (version 1.52r, Wayne Rasband, NIH, USA). The intensity ratio  
584 images between the PFO and the PtTFPP (FPFO/FPtTFPP) were calculated for all areas of  
585 the image with PFO and PtTFPP fluorescence above background noise and after background  
586 subtraction multiplied by 1000 to display on a 16bit scale (25). Measurements were then  
587 normalized to the baseline and processed in excel (Version 2016, Microsoft, USA) and  
588 Prism (version 5, GraphPad, USA).

589 **Acid phosphatase assay**

590 Acid phosphatase assay was used to measure cell number based on the conversion of pNPP to  
591 p-nitrophenol by cytosolic acid phosphatase (53). MCF7 clones were grown in a 24 well plate  
592 at a density of  $3 \times 10^4$  cells per well in either RPMI 1640 or SILAC medium (with dialysed  
593 FBS, 0.2 g/L arginine, 0.04 g/L lysine and 0.0053 g/L phenol red) with 2 mM glucose and no  
594 glutamine. After each time point (1, 2, 4, 6 days), medium was removed and each well was  
595 washed once with 200  $\mu$ L of 1X PBS. To each well, 100  $\mu$ L of assay buffer (0.1 M sodium  
596 acetate at pH 5.0, 0.1% Triton X-100, and 7.25 mM p-nitrophenyl phosphate) was added. The  
597 plates were then incubated at 37 °C for 2 h. The reaction was finally stopped with the addition  
598 of 50  $\mu$ L and color development was assayed at 405 nm using a Multiskan® EX plate reader.  
599 The non-enzymatic hydrolysis of the pNPP substrate was also determined by including wells  
600 with the assay buffer and without any cells. A standard curve, performed with the same assay  
601 and fixed number of cells (1000, 5000, 10000, 50000, 100000, 500000) was used to obtain  
602 the cell number from the different wells, using excel.

### 603 **BCL2 silencing**

604 For BCL2 proteins silencing experiments 100 ng of siRNA targeting BCL2 (Santa Cruz  
605 Biotechnology, sc-61899) or BCL(X)L (Santa Cruz Biotechnology, sc-43630) was  
606 transfected employing Lipofectamine. MCF7-pSFFV and MDA-231 cells were seeded at a  
607 density of  $2 \times 10^5$  in six-well plates to assess silencing efficiency by WB. After 24 hours  
608 incubation at 37 °C, cells were transfected as previously discussed. A siRNA consisting of a  
609 scrambled sequence was used a negative control (ctrl, Santa Cruz Biotechnology, sc-7007).  
610 One day following transfection, protein lysates were prepared from each well and stored at -  
611 80°C for further analysis. To assess the effect of BCL2 or BCL(X)L silencing on ATP  
612 production kinetics, cells were seeded on a glass wilco at a density of  $2 \times 10^3$  cells per dish,  
613 and allowed to adhere for 24 hours. Cells were then co-transfected with 100 ng of MitoAteam  
614 plasmid and 100ng of BCL2, BCL(X)L or control siRNA, as previously described. After 24

615 hours (48h for MDA-231), cells were prepared for time-lapse live cell imaging. To assess  
616 clonogenic ability and viability after BCL2 or BCL(X)L silencing, MCF7-pSFFV cells were  
617 seeded in a 6-well plate at a density of thousand cells per well and at a density of  $6 \times 10^4$  in 24-  
618 well plate for Annexin V/PI staining. Cells were incubated for 24 hours and transfected with  
619 100 ng of BCL2, BCL(X)L or control siRNA; in both cases wells treated with Lipofectamine  
620 2000 and no DNA were added to exclude any effect that transfection reagents might have on  
621 cell viability. Following 24 hours incubation, 2 mL of fresh medium was added to each 6-  
622 well plates and cells let to grow colonies for 7 days, while 24 well plates were to detect  
623 apoptosis rates with flow cytometry.

#### 624 **Wound healing assay**

625 Cells were seeded at a concentration of  $3 \times 10^4$  in sterile 24 well plates and let to adhere over-  
626 night. A 2 well insert from Ibidi was placed into each well, before seeding the cells. The  
627 following day the insert was carefully removed in order to have a clear separation to follow.  
628 All clones were imaged at selected timepoints (0, 24, 48 and 72 hours) on a Nikon TE2000  
629 microscope. Images were imported in ImageJ2; a Find Edges function followed by Sharpen  
630 was used to increase the contrast of the cell area compared to the wound. The LUT (lookup  
631 table) was inverted and the analyze particle function was used (size between 100000 and  
632 50000000, Circularity: 0.00-1.00) with Outlines showed to obtain the area of the wound. Data  
633 were then processed with excel.

#### 634 **RNA-seq experiments and gene expression analysis of publically available datasets**

635 MCF7 clones were seeded in t25 flasks and let adhere overnight. On the following day, cells  
636 were trypsinised, collected in eppendorf tubes and centrifuged. RNA was extracted with  
637 TRIzol reagent (ThermoFisher Scientific) and samples mechanically disrupted using a  
638 homogeniser. Subsequently, chloroform was added to separate an upper aqueous phase  
639 (containing RNA) from the rest. This was mixed with isopropanol and centrifuged at 12,000

640 x g at 4°C; the resulting pellet was put in 75% ethanol and centrifuged again at 7,500 x g at  
641 4°C. Pellet was let to air dry and resuspended in RNase free water for further quantification  
642 with Nanodrop 2000. Next, whole transcript RNA-seq was performed on the samples.  
643 Specifically, poly-A containing mRNA was purified from the RNA samples and RNA  
644 sequencing libraries were created using the KAPA stranded mRNAseq Kit (Illumina),  
645 according to the manufacturer’s instructions. Briefly, sequencing libraries were prepared by  
646 converting the RNA to cDNA followed by adapter ligation and enrichment of exon coding  
647 sequences by PCR using sequence-specific probes. The resulted cDNA libraries were  
648 sequenced on a HiSeq 4000 using a flow-cell generating 1 X 50 bp reads. Transcriptome  
649 profiles were created using an existing in-house bioinformatic pipeline. More specifically,  
650 after removing the optical duplicates with Clumpify and removing sequencing adapters, the  
651 reads were mapped to the human reference genome using TopHat-Bowtie and HTSeq-count  
652 was used to create gene-count matrices. Raw counts from RNA-seq experiments were  
653 normalized using DESeq2 (R library, version 1.26.0) (54) using ‘rlog’ as method and ‘~  
654 cell\_line’ as design formula. ENSEMBL ids were mapped to symbols with mygene (python  
655 package, version 3.1.0). Genes involved in the respiratory chain complexes I to V were  
656 retrieved from the “gene names” database curated by the HGNC - HUGO Gene  
657 Nomenclature Committee (<https://www.genenames.org/data/genegroup/#!/group/639>). Of the  
658 97 genes of interest, 96 were present in the dataset.

659 Table 1. Breakdown of genes included for each respiratory chain complex.

Complex	# genes
Complex I	44
Complex II	4
Complex III	10
Complex IV	19

660

661 Transcriptomic data from the Cancer Cell Line Encyclopedia (CCLE) were downloaded on  
662 2019-06-29 from the CCLE website (55). In downstream analyses, we focused on breast  
663 cancer cell lines (set to “BRCA”, n=50) and on genes (n=40) from the respiratory chain  
664 complexes found to be altered in the MCF7 clones. Transcriptomic data (RNASeq, FPKM)  
665 from patient-derived xenografts (PDXs) were downloaded from the supplementary materials  
666 of Gao *et al.*, (28). We restricted the analysis to untreated PDXs from breast cancer patients  
667 (n=38) and on genes from the respiratory chain complexes found to be altered in the MCF7  
668 clones (n=37 out of 40 were found with COX1, COX2 and COX3 missing). Transcriptomic  
669 data (mRNA z-Scores, Illumina Human v3 microarray) for n=1904 primary tumour samples  
670 from breast cancer patients from the “Molecular Taxonomy of Breast Cancer International  
671 Consortium” (METABRIC) (56) study were downloaded on 2020-08-07 from the cBioportal  
672 website ([https://www.cbioportal.org/study/summary?id=brca\\_metabric](https://www.cbioportal.org/study/summary?id=brca_metabric)). Downstream  
673 analyses included genes from the respiratory chain complexes found to be altered in the  
674 MCF7 clones (n=36 out of 40 were found with NDUFS1, COX1, COX2 and COX3 missing).  
675 We investigated the dependency of the respiratory chain complexes by BCL2 family  
676 members by comparing the expression of the mitochondrial genes listed above in parental  
677 (pSFFV) and BCL2 or BCL(X)L overexpressing MCF7 clones. We fitted univariate  
678 regression models and we evaluated statistical significance with overall ANOVA p-values.  
679 We did not adjust p-values for multiple comparisons as these analyses were considered  
680 exploratory. We reported pairwise cell line comparisons by TukeyHSD Post-Hoc tests and  
681 mean expression difference, 95% confidence intervals (CI, lower and upper) and p-values  
682 (Supplementary Table 1). Next, we examined the association between BCL2 genes (BCL2 or  
683 BCL2L1) and those mitochondrial genes found to be differential expressed in the MCF7

684 clones to examine whether these findings are generalizable to other cell lines, PDX models  
685 and patient tumour samples. We reported Spearman correlation as an effect size metric and  
686 corresponding p-values in Supplementary Table 2.

### 687 **Data and Code availability**

688 The raw and processed RNA sequencing data for the MCF7 cell lines generated in this study  
689 are publicly available in GEO (reference number GSE158808). Data, processing and analysis  
690 code for the transcriptomic-based analysis is publicly available and archived at Zenodo  
691 (<https://doi.org/10.5281/zenodo.4058036>).

### 692 **Statistical analysis**

693 Data are given as means  $\pm$  S.D. (standard deviation). The number of independent experiments  
694 performed is indicated in the figure legends (from 3 to 5). The variance was assumed to be  
695 similar between the compared groups with a normal distribution. For statistical comparison,  
696 two-way analysis of variance (ANOVA) or one-way analysis followed by Tukey's post hoc  
697 test were employed. p-values  $< 0.05$  were considered to be statistically significant

698  
699 Supplementary information is available at Cell Death and Differentiation's website.

### 700 **REFERENCES**

- 701 1. Czabotar PE, Lessene G, Strasser A, Adams JM. Control of apoptosis by the BCL-2 protein  
702 family: implications for physiology and therapy. *Nat Rev Mol Cell Biol.* 2014;15(1):49-63.
- 703 2. Aouacheria A, Baghdiguian S, Lamb HM, Huska JD, Pineda FJ, Hardwick JM. Connecting  
704 mitochondrial dynamics and life-or-death events via Bcl-2 family proteins. *Neurochem Int.*  
705 2017;109:141-61.
- 706 3. Autret A, Martin SJ. Emerging role for members of the Bcl-2 family in mitochondrial  
707 morphogenesis. *Mol Cell.* 2009;36(3):355-63.
- 708 4. Gross A, Katz SG. Non-apoptotic functions of BCL-2 family proteins. *Cell Death Differ.*  
709 2017;24(8):1348-58.
- 710 5. Rolland SG, Conradt B. New role of the BCL2 family of proteins in the regulation of  
711 mitochondrial dynamics. *Curr Opin Cell Biol.* 2010;22(6):852-8.
- 712 6. Westermann B. Bioenergetic role of mitochondrial fusion and fission. *Biochim Biophys Acta.*  
713 2012;1817(10):1833-8.
- 714 7. Brenner C, Cadiou H, Vieira HL, Zamzami N, Marzo I, Xie Z, et al. Bcl-2 and Bax regulate the  
715 channel activity of the mitochondrial adenine nucleotide translocator. *Oncogene.* 2000;19(3):329-  
716 36.

- 717 8. Vander Heiden MG, Li XX, Gottlieb E, Hill RB, Thompson CB, Colombini M. Bcl-xL promotes  
718 the open configuration of the voltage-dependent anion channel and metabolite passage through the  
719 outer mitochondrial membrane. *J Biol Chem.* 2001;276(22):19414-9.
- 720 9. Alavian KN, Li H, Collis L, Bonanni L, Zeng L, Sacchetti S, et al. Bcl-xL regulates metabolic  
721 efficiency of neurons through interaction with the mitochondrial F1FO ATP synthase. *Nat Cell Biol.*  
722 2011;13(10):1224-33.
- 723 10. Chen YB, Aon MA, Hsu YT, Soane L, Teng X, McCaffery JM, et al. Bcl-xL regulates  
724 mitochondrial energetics by stabilizing the inner membrane potential. *J Cell Biol.* 2011;195(2):263-  
725 76.
- 726 11. Perciavalle RM, Stewart DP, Koss B, Lynch J, Milasta S, Bathina M, et al. Anti-Apoptotic MCL-  
727 1 Localizes to the Mitochondrial Matrix and Couples Mitochondrial Fusion to Respiration. *Nature Cell*  
728 *Biology.* 2012;14(6):575-83.
- 729 12. Boroughs LK, DeBerardinis RJ. Metabolic pathways promoting cancer cell survival and  
730 growth. *Nat Cell Biol.* 2015;17(4):351-9.
- 731 13. Mason EF, Rathmell JC. Cell metabolism: an essential link between cell growth and  
732 apoptosis. *Biochimica et biophysica acta.* 2011;1813(4):645-54.
- 733 14. Dawson SJ, Makretsov N, Blows FM, Driver KE, Provenzano E, Le Quesne J, et al. BCL2 in  
734 breast cancer: a favourable prognostic marker across molecular subtypes and independent of  
735 adjuvant therapy received. *Br J Cancer.* 2010;103(5):668-75.
- 736 15. Keitel U, Scheel A, Thomale J, Halpape R, Kaulfuss S, Scheel C, et al. Bcl-xL mediates  
737 therapeutic resistance of a mesenchymal breast cancer cell subpopulation. *Oncotarget.*  
738 2014;5(23):11778-91.
- 739 16. Lindner AU, Lucantoni F, Varešlija D, Resler A, Murphy BM, Gallagher WM, et al. Low cleaved  
740 caspase-7 levels indicate unfavourable outcome across all breast cancers. *J Mol Med (Berl).*  
741 2018;96(10):1025-37.
- 742 17. Antonietti P, Gessler F, Dussmann H, Reimertz C, Mittelbronn M, Prehn JH, et al. AT-101  
743 simultaneously triggers apoptosis and a cytoprotective type of autophagy irrespective of expression  
744 levels and the subcellular localization of Bcl-xL and Bcl-2 in MCF7 cells. *Biochim Biophys Acta.*  
745 2016;1863(4):499-509.
- 746 18. Delgado ME, Olsson M, Lincoln FA, Zhivotovsky B, Rehm M. Determining the contributions of  
747 caspase-2, caspase-8 and effector caspases to intracellular VDVADase activities during apoptosis  
748 initiation and execution. *Biochimica et Biophysica Acta (BBA) - Molecular Cell Research.*  
749 2013;1833(10):2279-92.
- 750 19. Laussmann MA, Passante E, Dussmann H, Rauen JA, Wurstle ML, Delgado ME, et al.  
751 Proteasome inhibition can induce an autophagy-dependent apical activation of caspase-8. *Cell Death*  
752 *Differ.* 2011;18(10):1584-97.
- 753 20. Lindner AU, Concannon CG, Boukes GJ, Cannon MD, Llambi F, Ryan D, et al. Systems analysis  
754 of BCL2 protein family interactions establishes a model to predict responses to chemotherapy.  
755 *Cancer Res.* 2013;73(2):519-28.
- 756 21. Popgeorgiev N, Jabbour L, Gillet G. Subcellular Localization and Dynamics of the Bcl-2 Family  
757 of Proteins. *Front Cell Dev Biol.* 2018;6:13.
- 758 22. Imamura H, Huynh Nhat KP, Togawa H, Saito K, Iino R, Kato-Yamada Y, et al. Visualization of  
759 ATP levels inside single living cells with fluorescence resonance energy transfer-based genetically  
760 encoded indicators. *Proceedings of the National Academy of Sciences of the United States of*  
761 *America.* 2009;106(37):15651-6.
- 762 23. D'Orsi B, Kilbride SM, Chen G, Perez Alvarez S, Bonner HP, Pfeiffer S, et al. Bax regulates  
763 neuronal Ca<sup>2+</sup> homeostasis. *J Neurosci.* 2015;35(4):1706-22.
- 764 24. Dussmann H, Rehm M, Kögel D, Prehn JH. Outer mitochondrial membrane permeabilization  
765 during apoptosis triggers caspase-independent mitochondrial and caspase-dependent plasma  
766 membrane potential depolarization: a single-cell analysis. *J Cell Sci.* 2003;116(Pt 3):525-36.



- 767 25. Düssmann H, Perez-Alvarez S, Anilkumar U, Papkovsky DB, Prehn JH. Single-cell time-lapse  
768 imaging of intracellular O(2) in response to metabolic inhibition and mitochondrial cytochrome-c  
769 release. *Cell Death Dis.* 2017;8(6):e2853.
- 770 26. Fercher A, O'Riordan TC, Zhdanov AV, Dmitriev RI, Papkovsky DB. Imaging of cellular oxygen  
771 and analysis of metabolic responses of mammalian cells. *Methods Mol Biol.* 2010;591:257-73.
- 772 27. Lucantoni F, Lindner AU, O'Donovan N, Dussmann H, Prehn JHM. Systems modeling  
773 accurately predicts responses to genotoxic agents and their synergism with BCL-2 inhibitors in triple  
774 negative breast cancer cells. *Cell Death & Disease.* 2018;9.
- 775 28. Gao H, Korn JM, Ferretti S, Monahan JE, Wang Y, Singh M, et al. High-throughput screening  
776 using patient-derived tumor xenografts to predict clinical trial drug response. *Nat Med.*  
777 2015;21(11):1318-25.
- 778 29. Oakes SR, Vaillant F, Lim E, Lee L, Breslin K, Feleppa F, et al. Sensitization of BCL-2-expressing  
779 breast tumors to chemotherapy by the BH3 mimetic ABT-737. *Proc Natl Acad Sci U S A.*  
780 2012;109(8):2766-71.
- 781 30. Vaillant F, Merino D, Lee L, Breslin K, Pal B, Ritchie ME, et al. Targeting BCL-2 with the BH3  
782 mimetic ABT-199 in estrogen receptor-positive breast cancer. *Cancer Cell.* 2013;24(1):120-9.
- 783 31. Ashton TM, McKenna WG, Kunz-Schughart LA, Higgins GS. Oxidative Phosphorylation as an  
784 Emerging Target in Cancer Therapy. *Clin Cancer Res.* 2018;24(11):2482-90.
- 785 32. Chandel NS. Mitochondria and cancer. *Cancer Metab.* 2014;2:8-.
- 786 33. Diers AR, Broniowska KA, Chang C-F, Hogg N. Pyruvate fuels mitochondrial respiration and  
787 proliferation of breast cancer cells: effect of monocarboxylate transporter inhibition. *The*  
788 *Biochemical journal.* 2012;444(3):561-71.
- 789 34. Huang H, Hu X, Eno CO, Zhao G, Li C, White C. An interaction between Bcl-xL and the voltage-  
790 dependent anion channel (VDAC) promotes mitochondrial Ca<sup>2+</sup> uptake. *J Biol Chem.*  
791 2013;288(27):19870-81.
- 792 35. Shimizu S, Konishi A, Kodama T, Tsujimoto Y. BH4 domain of antiapoptotic Bcl-2 family  
793 members closes voltage-dependent anion channel and inhibits apoptotic mitochondrial changes and  
794 cell death. *Proceedings of the National Academy of Sciences of the United States of America.*  
795 2000;97(7):3100-5.
- 796 36. Schendel SL, Montal M, Reed JC. Bcl-2 family proteins as ion-channels. *Cell Death &*  
797 *Differentiation.* 1998;5(5):372-80.
- 798 37. Vander Heiden MG, Chandel NS, Williamson EK, Schumacker PT, Thompson CB. Bcl-xL  
799 Regulates the Membrane Potential and Volume Homeostasis of Mitochondria. *Cell.* 1997;91(5):627-  
800 37.
- 801 38. Stein LR, Imai S-i. The dynamic regulation of NAD metabolism in mitochondria. *Trends in*  
802 *endocrinology and metabolism: TEM.* 2012;23(9):420-8.
- 803 39. Bonuccelli G, De Francesco EM, de Boer R, Tanowitz HB, Lisanti MP. NADH autofluorescence,  
804 a new metabolic biomarker for cancer stem cells: Identification of Vitamin C and CAPE as natural  
805 products targeting "stemness". *Oncotarget.* 2017;8(13):20667-78.
- 806 40. Zhu L, Yu Y, Chua BH, Ho YS, Kuo TH. Regulation of sodium-calcium exchange and  
807 mitochondrial energetics by Bcl-2 in the heart of transgenic mice. *J Mol Cell Cardiol.*  
808 2001;33(12):2135-44.
- 809 41. Imahashi K, Schneider MD, Steenbergen C, Murphy E. Transgenic expression of Bcl-2  
810 modulates energy metabolism, prevents cytosolic acidification during ischemia, and reduces  
811 ischemia/reperfusion injury. *Circ Res.* 2004;95(7):734-41.
- 812 42. Veatch JR, McMurray MA, Nelson ZW, Gottschling DE. Mitochondrial dysfunction leads to  
813 nuclear genome instability via an iron-sulfur cluster defect. *Cell.* 2009;137(7):1247-58.
- 814 43. Geissler A, Krimmer T, Bömer U, Guiard B, Rassow J, Pfanner N. Membrane Potential-Driven  
815 Protein Import into Mitochondria: The Sorting Sequence of Cytochrome b(2) Modulates the  $\Delta\psi$ -  
816 Dependence of Translocation of the Matrix-targeting Sequence. *Molecular Biology of the Cell.*  
817 2000;11(11):3977-91.

- 818 44. Martinez-Reyes I, Diebold LP, Kong H, Schieber M, Huang H, Hensley CT, et al. TCA Cycle and  
819 Mitochondrial Membrane Potential Are Necessary for Diverse Biological Functions. *Mol Cell*.  
820 2016;61(2):199-209.
- 821 45. Bernal SD, Lampidis TJ, Summerhayes IC, Chen LB. Rhodamine-123 selectively reduces clonal  
822 growth of carcinoma cells in vitro. *Science*. 1982;218(4577):1117-9.
- 823 46. Summerhayes IC, Lampidis TJ, Bernal SD, Nadakavukaren JJ, Nadakavukaren KK, Shepherd  
824 EL, et al. Unusual retention of rhodamine 123 by mitochondria in muscle and carcinoma cells. *Proc*  
825 *Natl Acad Sci U S A*. 1982;79(17):5292-6.
- 826 47. Houston MA, Augenlicht LH, Heerdt BG. Stable Differences in Intrinsic Mitochondrial  
827 Membrane Potential of Tumor Cell Subpopulations Reflect Phenotypic Heterogeneity. *International*  
828 *Journal of Cell Biology*. 2011;2011:11.
- 829 48. Chen ZX, Pervaiz S. Bcl-2 induces pro-oxidant state by engaging mitochondrial respiration in  
830 tumor cells. *Cell Death Differ*. 2007;14(9):1617-27.
- 831 49. Geissmann Q. OpenCFU, a new free and open-source software to count cell colonies and  
832 other circular objects. *PLoS One*. 2013;8(2):e54072.
- 833 50. Frezza C, Cipolat S, Scorrano L. Organelle isolation: functional mitochondria from mouse  
834 liver, muscle and cultured fibroblasts. *Nat Protocols*. 2007;2(2):287-95.
- 835 51. Fercher A, Borisov SM, Zhdanov AV, Klimant I, Papkovsky DB. Intracellular O<sub>2</sub> sensing probe  
836 based on cell-penetrating phosphorescent nanoparticles. *ACS Nano*. 2011;5(7):5499-508.
- 837 52. Kondrashina AV, Dmitriev RI, Borisov SM, Klimant I, O'Brien I, Nolan YM, et al. A  
838 Phosphorescent Nanoparticle-Based Probe for Sensing and Imaging of (Intra)Cellular Oxygen in  
839 Multiple Detection Modalities. *Advanced Functional Materials*. 2012;22(23):4931-9.
- 840 53. Yang TT, Sinai P, Kain SR. An acid phosphatase assay for quantifying the growth of adherent  
841 and nonadherent cells. *Anal Biochem*. 1996;241(1):103-8.
- 842 54. Love MI, Huber W, Anders S. Moderated estimation of fold change and dispersion for RNA-  
843 seq data with DESeq2. *Genome Biology*. 2014;15(12):550.
- 844 55. Barretina J, Caponigro G, Stransky N, Venkatesan K, Margolin AA, Kim S, et al. The Cancer  
845 Cell Line Encyclopedia enables predictive modelling of anticancer drug sensitivity. *Nature*.  
846 2012;483(7391):603-7.
- 847 56. Curtis C, Shah SP, Chin SF, Turashvili G, Rueda OM, Dunning MJ, et al. The genomic and  
848 transcriptomic architecture of 2,000 breast tumours reveals novel subgroups. *Nature*.  
849 2012;486(7403):346-52.

## 850 **Figure Legend**

### 851 **Figure 1. Characterisation of MCF7 clones.**

852 **(A)** Representative WB for MCF7 cell lines. Cells were lysed and analysed by  
853 immunoblotting to detect levels of two pro-apoptotic protein, BAX and BAK, and three anti-  
854 apoptotic protein, BCL2, BCL(X)L and MCL1. Actin was used as loading control to  
855 normalize protein concentration values post densitometry and HeLa cell line lysates were  
856 used for absolute quantification. **(B)** Expression levels for BCL2 proteins as determined by  
857 comparing densitometric signals and considering absolute quantification levels in HeLa cells.  
858 Data represent mean  $\pm$  SD from n=3 independent experiments and quantifications were

859 analysed by two-way ANOVA with Tukey post-test (\* indicates a p-value < 0.5, \*\* indicates  
860 a p-value < 0.01, \*\*\* indicates a p-value < 0.001). (C) Immunofluorescence staining showing  
861 localization of BCL2 and BCL(X)L, respectively. MCF7-BCL2 and BCL(X)L  
862 overexpressing cells were fixed with paraformaldehyde (4% PFA) and permeabilised with a  
863 solution of 95% ethanol and 5% glacial acetic acid. DAPI was used to visualize nuclei while  
864 MitoTracker Red CMXRos was used to stain mitochondria. Images are representative of  
865 immunofluorescence performed on n=3 independent cultures. (D) Percentages of surviving  
866 cells (Annexin V-/PI- fraction) following 24 hours control, STS (2  $\mu$ M) or Cisplatin (40  $\mu$ M)  
867 treatment. (E) Percentages of apoptotic cells (sum of Annexin V+/PI- and Annexin V+/PI+  
868 fractions) post treatments. Significance was assessed with a two-way ANOVA and Tukey  
869 post-test (\* indicates a p-value < 0.05, \*\* indicates a p-value < 0.01, \*\*\* indicates a p-value  
870 < 0.001). Column represents mean  $\pm$  SD for n = 3 experiments.

871 **Figure 2. MCF7-BCL2 and BCL(X)L clones produces similar amounts of mitochondrial**  
872 **ATP by producing/consuming less NAD(P)H, when compared to MCF7-pSFFV cells.**

873 (A) Representative traces of mitochondrial ATP signal and mitochondrial membrane  
874 potential. FRET/CFP ratio kinetics and TMRM fluorescence were monitored simultaneously  
875 in all MCF7 clones. Cells were starved for three hours; after that, the baseline was recorded  
876 for 20 minutes and 2 mM sodium pyruvate was added into the medium. Following 20  
877 minutes treatment, 10  $\mu$ M of oligomycin was supplemented for the last 20 minutes. All data  
878 represent mean  $\pm$  SD from n=4-5 independent experiments and both signals are normalized to  
879 the baseline levels (each cell line normalised to its own baseline). (B) The absolute  
880 FRET/CFP ratio were analysed by taking into account the maximal value reached by the  
881 probe after pyruvate addition and minimal value after oligomycin treatment. Box and  
882 whiskers represents single cell values from all experiments. (C) TMRM intensity values,  
883 normalised to the baseline levels from TMRM kinetics, were analysed by taking into account

884 the maximal value reached following each treatment. **(D)** TMRM fluorescence absolute  
885 values obtained from baseline. Box and whiskers represents single cell values from all  
886 experiments. All values were analysed by two-way ANOVA with Tukey post-test (\*  
887 indicates a p-value < 0.05, \*\* indicates a pvalue < 0.01 \*\*\* indicates a p-value < 0.001). **(E)**  
888 Representative traces of mitochondrial NAD(P)H signal. NAD(P)H autofluorescence was  
889 monitored in all MCF7 clones, by following similar experimental protocol as above. All data  
890 represent mean  $\pm$  SD from n=3 independent experiments and signals are normalized to the  
891 baseline levels (each cell line normalised to its own baseline). **(F)** The absolute NAD(P)H  
892 fluorescence was analysed by taking into account the maximal autofluorescence value  
893 reached after treatments. Box and whiskers represents single cell values from all experiments.  
894 **(G)** NAD(P)H curve fitting for pyruvate addition was calculated using a fit function in  
895 GraphPad Prism. **(H)** NAD(P)H/ATP ratio, calculated by dividing NAD(P)H absolute  
896 fluorescence to absolute mitoAteam FRET/CFP ratio. All values were analysed by two-way  
897 ANOVA with Tukey post-test (\* indicates a pvalue < 0.05, \*\* indicates a p-value < 0.01 \*\*\*  
898 indicates a p-value < 0.001).

899 **Figure 3. BCL2 and BCL(X)L cells maintain higher mitochondrial ATP after**  
900 **oligomycin titration.**

901 **(A)** Representative traces of mitochondrial ATP signal and mitochondrial membrane  
902 potential. FRET/CFP ratio kinetics and TMRM fluorescence were monitored simultaneously  
903 in all MCF7 clones. Cells were placed in KB with 2 mM pyruvate; baseline was recorded for  
904 20 minutes and oligomycin titration started by adding 1 nM, 10 nM and 100 nM of the drug  
905 with an interval of 20 minutes for each concentration. All data represent mean  $\pm$  SD from n=3  
906 independent experiments and both signals are normalized to the baseline levels (each cell line  
907 normalised to its own baseline). **(B)** The absolute FRET/CFP ratio were analysed by taking  
908 into account the minimal value reached by the probe after each addition. **(C)** Slope values of

909 oligomycin titration were assessed by dividing the  $\Delta$ FRET/CFP ratio to the  $\Delta$ time (time  
910 offset – time onset). Box and whiskers represents single cell values from all experiments. **(D)**  
911 TMRM intensity values normalised to the baseline levels from TMRM kinetics were  
912 analysed by taking into account the maximal value reached after each treatment. All values  
913 were analysed by two-way ANOVA with Tukey post-test (\* indicates a pvalue < 0.05, \*\*  
914 indicates a p-value < 0.01 \*\*\* indicates a p-value < 0.001). **(E)** TMRM fluorescence absolute  
915 values obtained from baseline. **(F)** Protein levels for ATP synthase subunit  $\beta$  in MCF7 clones  
916 were obtained from cell lysates and normalized to actin. **(G)** A commercially available kit  
917 from Abcam was used after isolation of mitochondrial fraction from MCF7 cell lines, to  
918 calculate the activity of ATP synthase. In order to account for protein concentration, the  
919 activity was normalized to ATP synthase subunit  $\beta$ . All data represent mean  $\pm$  SD from 3  
920 independent experiments. All values were analysed by one-way ANOVA with Tukey post-  
921 test.

922 **Figure 4. BCL2 and BCL(X)L cells maintain higher cytosolic ATP during starvation.**

923 **(A)** Representative traces of cytosolic ATP signal and mitochondrial membrane potential.  
924 FRET/CFP ratio from ATeam probe and TMRM fluorescence were monitored  
925 simultaneously in all MCF7-ATeam clones. Cells were placed in KB with no nutrients and  
926 signal recorded every 5 minutes. After 23 hours, 5 mM glucose was supplemented for the  
927 remaining hour. All data represent mean  $\pm$  SD from n=3 independent experiments and both  
928 signals are normalized to the baseline levels (each cell line normalised to its own baseline).  
929 **(B)** The absolute FRET/CFP ratio were analysed by taking into account the minimal value  
930 reached by the probe at each time-point selected. **(C)** Slope values of the decrease in  
931 cytosolic ATP, during starvation, were assessed by dividing the  $\Delta$ FRET/CFP ratio to the  
932  $\Delta$ time (time offset – time onset), at the indicated time-points. All values were analysed by  
933 two-way ANOVA with Tukey post-test (\* indicates a p-value < 0.05, \*\* indicates a p-value <

934 0.01 \*\*\* indicates a p-value < 0.001). **(D)** Clonogenic assay of MCF7 clones in full medium  
935 (NT), starvation medium (SILAC medium plus dialysed FBS with no glucose and no  
936 glutamine) and reduced glucose medium (SILAC medium plus dialysed FBS with 5mM  
937 glucose and no glutamine). In the case of starvation, the medium was replaced with full  
938 RPMI after 24 h. Clonogenic potential was assayed after 7 days in culture. **(E)** Colonies were  
939 counted using OpenCFU software and the change in colony growth was normalized to non-  
940 treated (NT) MCF7-pSFFV cells. **(F)** Percentages of surviving cells (Annexin V-/PI-  
941 fraction) in non-treated (NT), starved and reduced glucose conditions. Bars represent means  $\pm$   
942 SD from three independent experiments. One-way ANOVA with Tukey post-test was used to  
943 assess significance (\* indicated a p-value < 0.05, \*\* indicates a p-value < 0.01, \*\*\* indicates  
944 a p-value < 0.001).

945 **Figure 5. BCL2 and BCL(X)L maintain higher cytosolic ATP after sodium azide**  
946 **treatment and regulate oxygen consumption during hypoxia.**

947 **(A)** Representative traces of cytosolic ATP signal and mitochondrial membrane potential.  
948 FRET/CFP ratio kinetics from ATeam probe and TMRM fluorescence were monitored, in all  
949 MCF7-ATeam clones. Cells were placed in KB with pyruvate; baseline was recorded for 20  
950 minutes and 0.1 mM NaAzide was added into the medium. After 30 minutes treatment, 5 mM  
951 glucose was supplemented for the last 20 minutes. All data represent mean  $\pm$  SD from n=3  
952 independent experiments and both signals are normalized to the baseline levels (each cell line  
953 normalised to its own baseline). **(B)** The absolute FRET/CFP ratio were analysed by taking  
954 into account the minimal value reached by the probe after NaAzide addition and maximal  
955 value after glucose addition. **(C)** TMRM intensity values normalised to the baseline levels  
956 from TMRM kinetics were analysed by taking into account the maximal value reached after  
957 each treatment. **(D)** Slope values of sodium azide addition were assessed by dividing the  
958  $\Delta$ FRET/CFP ratio to the  $\Delta$ time (time offset – time onset). All values were analysed by two-

959 way ANOVA with Tukey post-test (\* indicates a p-value < 0.05, \*\* indicates a p-value <  
960 0.01 \*\*\* indicates a p-value < 0.001). (E) Kinetics of intracellular oxygen levels were  
961 measured with MitoImage™ (MM2) and normalised to baseline at 21% O<sub>2</sub>. After reduction  
962 of the atmospheric O<sub>2</sub> from 21 to 2% cells were treated with 10 μM oligomycin and 5 mM  
963 glucose followed by 10 μM FCCP and the atmospheric O<sub>2</sub> was set back to 21% before the  
964 end of the experiment in all MCF7 clones, as indicated on top of the left graph for MCF7-  
965 pSFFV. All data represent mean ± SD from a minimum of 3 independent experiments. (F)  
966 Area above baseline (at 2% oxygen) for oligomycin + glucose and FCCP treatments.  
967 Addition of oligomycin and glucose inhibit mitochondrial ATP synthesis; with the increase of  
968 the intracellular O<sub>2</sub>, the O<sub>2</sub> consumption in BCL2 and BCL(X)L overexpressing cells was  
969 decreased, due to the activity of the ATP synthase, than in the pSFFV clone. One-way  
970 ANOVA with Tukey post-test was used to assess significance (\* indicated a p-value < 0.05,  
971 \*\* indicates a p-value < 0.01, \*\*\* indicates a p-value < 0.001). (G) Clonogenic assay of  
972 MCF7 clones in full RPMI medium (11 mM glucose) and SILAC medium plus dialysed FBS  
973 and 2 mM or 5 mM glucose, respectively, in hypoxic conditions (1% oxygen). Colonies were  
974 counted using OpenCFU software and the change in colony growth was normalized to non-  
975 treated (NT) MCF7-pSFFV cells. All values were analysed by two-way ANOVA with Tukey  
976 post-test (\* indicates a p-value < 0.05, \*\* indicates a p-value < 0.01 \*\*\* indicates a p-value <  
977 0.001). Bars represent means ± SD from three independent experiments

978 **Figure 6. BCL2 and BCL(X)L silencing decreases ATP production following pyruvate**  
979 **addition and decrease clonogenic potential.**

980 (A) Representative traces of mitochondrial ATP signal and mitochondrial membrane  
981 potential in siRNA co-transfected cells. FRET/CFP ratio kinetics from mitoATeam probe and  
982 TMRM fluorescence were monitored simultaneously in MCF7-pSFFV. Cells were starved  
983 for three hours; after that a baseline was recorded for 20 minutes and 2 mM sodium pyruvate

984 was added into the medium. After 20 minutes treatment, 10  $\mu$ M of oligomycin was  
985 supplemented for the last 20 minutes. All data represent mean  $\pm$  SD from n=3 independent  
986 experiments and both signals are normalized to the baseline levels (each cell line normalised  
987 to its own baseline). **(B)** The absolute FRET/CFP ratio were analysed by taking into account  
988 the maximal value reached by the probe after pyruvate addition and minimal value after  
989 oligomycin. **(C)** TMRM intensity values normalised to the baseline levels from TMRM  
990 kinetics were analysed by taking into account the maximal value reached after each  
991 treatment. **(D)** TMRM fluorescence absolute values obtained from baseline. All values were  
992 analysed by two-way ANOVA with Tukey post-test (\* indicates a p-value < 0.05, \*\*  
993 indicates a p-value < 0.01 \*\*\* indicates a p-value < 0.001). **(E)** Clonogenic assay of MCF7  
994 cells treated with control, BCL2 or BCL(X)L siRNA and Lipofectamine in full medium.  
995 Clonogenic potential was assessed after 7 days in culture. **(F)** Colonies were counted  
996 automatically with OpenCFU and the change in colony growth was normalized to control  
997 siRNA treated cells. **(G)** Percentages of surviving cells (Annexin V-/PI- fraction) in same  
998 conditions. Bars represent means  $\pm$  SD from n=3 independent experiments. One-way  
999 ANOVA with Tukey post-test was used to assess significance (\* indicated a pvalue < 0.05,  
1000 \*\* indicates a p-value < 0.01, \*\*\* indicates a p-value < 0.001).

1001 **Figure 7. BCL2 and BCL(X)L overexpression increase proliferation and migration**  
1002 **properties in glucose limiting conditions.**

1003 **(A and B)** Cell numbers obtained from acid phosphatase assay for MCF7 clones in full RPMI  
1004 (11 mM glucose) and SILAC medium plus dialysed FBS with 2 mM glucose, respectively.  
1005 **(C and D)** Wound healing assay for MCF7 clones in full RPMI (11 mM glucose) and SILAC  
1006 medium plus dialysed FBS with 2 mM glucose, respectively. Bars represent means  $\pm$  SD  
1007 from n=3 independent experiments. All values were analysed by two-way ANOVA with



1008 Tukey post-test (\* indicates a p-value < 0.05, \*\* indicates a p-value < 0.01 \*\*\* indicates a p-  
1009 value < 0.001).

1010 **Figure 8. Gene expression analysis of respiratory chain in relation to BCL2 and**  
1011 **BCL(X)L in MCF7 clones, CCLE and METABRIC datasets.**

1012 Comparison between expression of the genes from the respiratory chain, grouped by  
1013 complex. For the in-house dataset, the relative gene levels, expressed as rlog normalized and  
1014 z-scored values, for the control, BCL2 and BCL(X)L overexpressing clones (in duplicates,  
1015 R1 and R2) are size- and color-coded (lower in blue, higher in red). Only genes that were  
1016 statistically significantly different (non-adjusted p-values < 0.05; n=40 out of n=96 tested  
1017 genes) are included in the figure. The statistical output including the effect size and  
1018 comparison between individual cell lines for the complete set of genes that mapped to the  
1019 complexes (n=96) are reported in the Supplementary Table 1. For the other datasets, we used  
1020 the expression at the transcript level (BCL2 and BCL2L1). The association effect size  
1021 expressed as Spearman correlation between BCL2 or BCL(X)L and each gene was size- and  
1022 color-coded similarly to the data from the MCF7 clones to facilitate comparison. Genes with  
1023 statistically significant correlation with BCL2 or BCL(X)L expression were annotated in the  
1024 figure. The statistical output including effect size and p-values (unadjusted) for all the tested  
1025 genes are included in the Supplementary table 2. For the CCLE, METABRIC data sets (Fig.  
1026 8) and Gao PDXs (Supplementary Fig. 11) positive correlation is indicated in a bigger red dot  
1027 and negative correlation with a smaller blue dot.

1028

# Figure 1

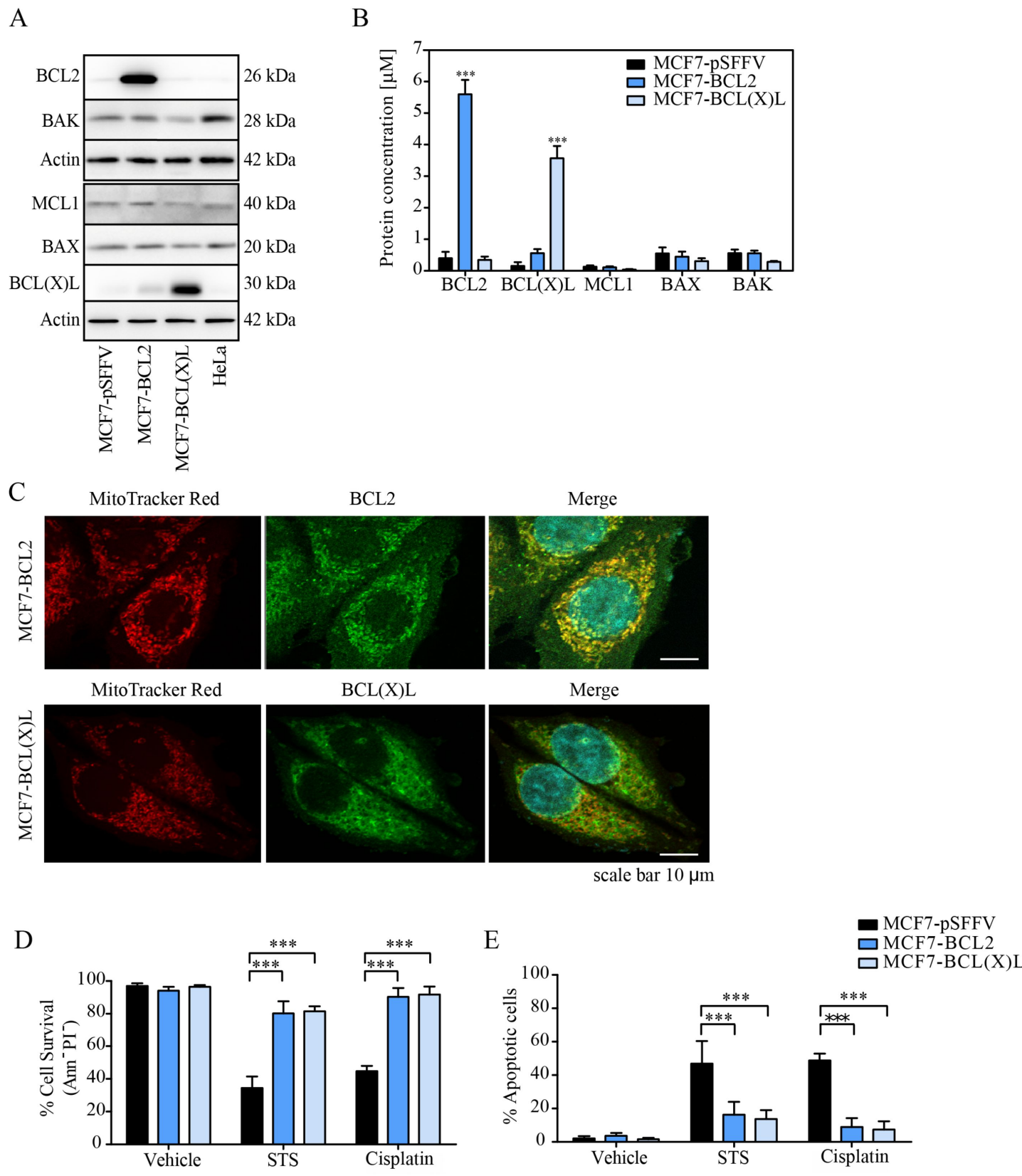


# Figure 2

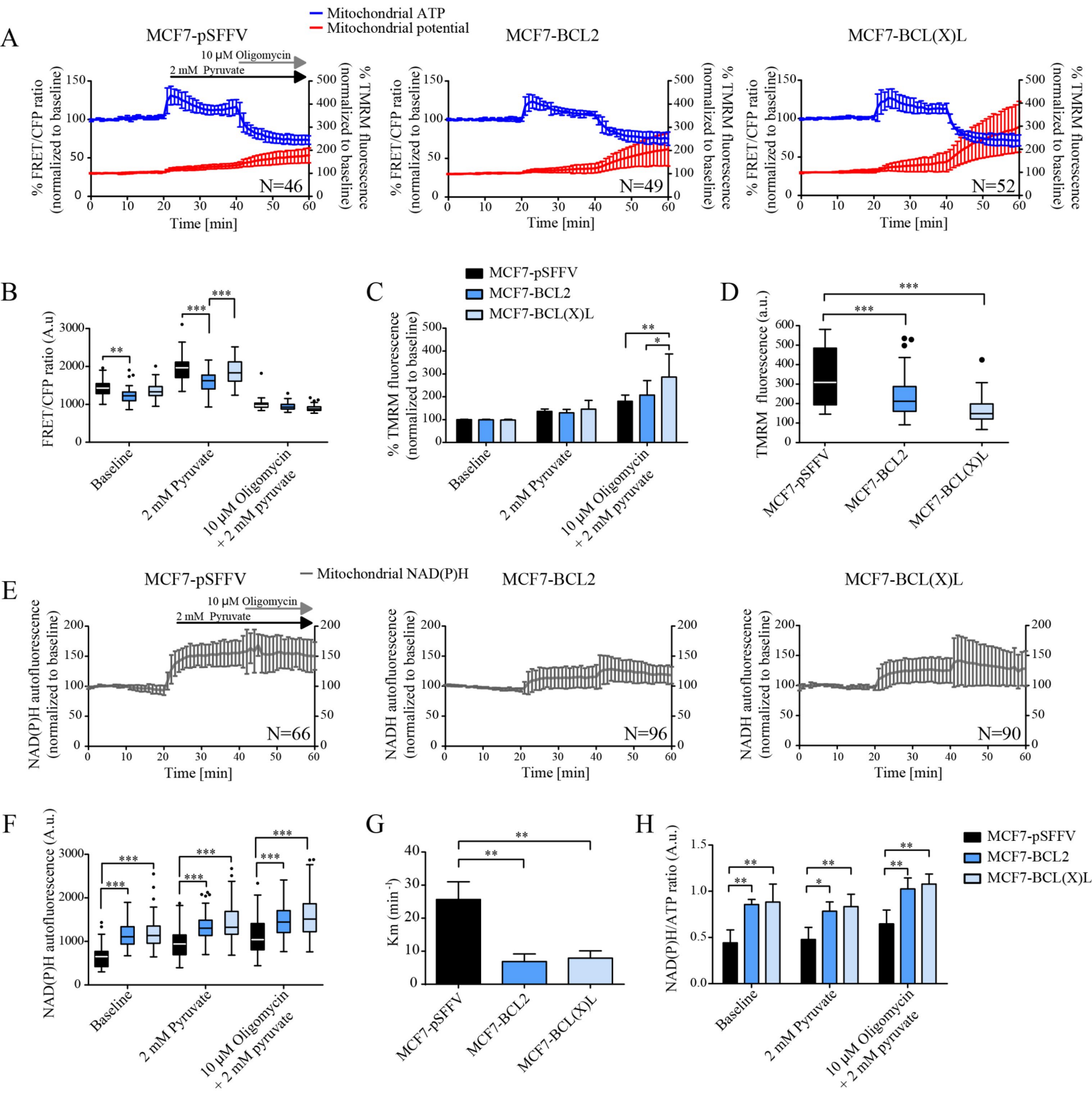


# Figure 3

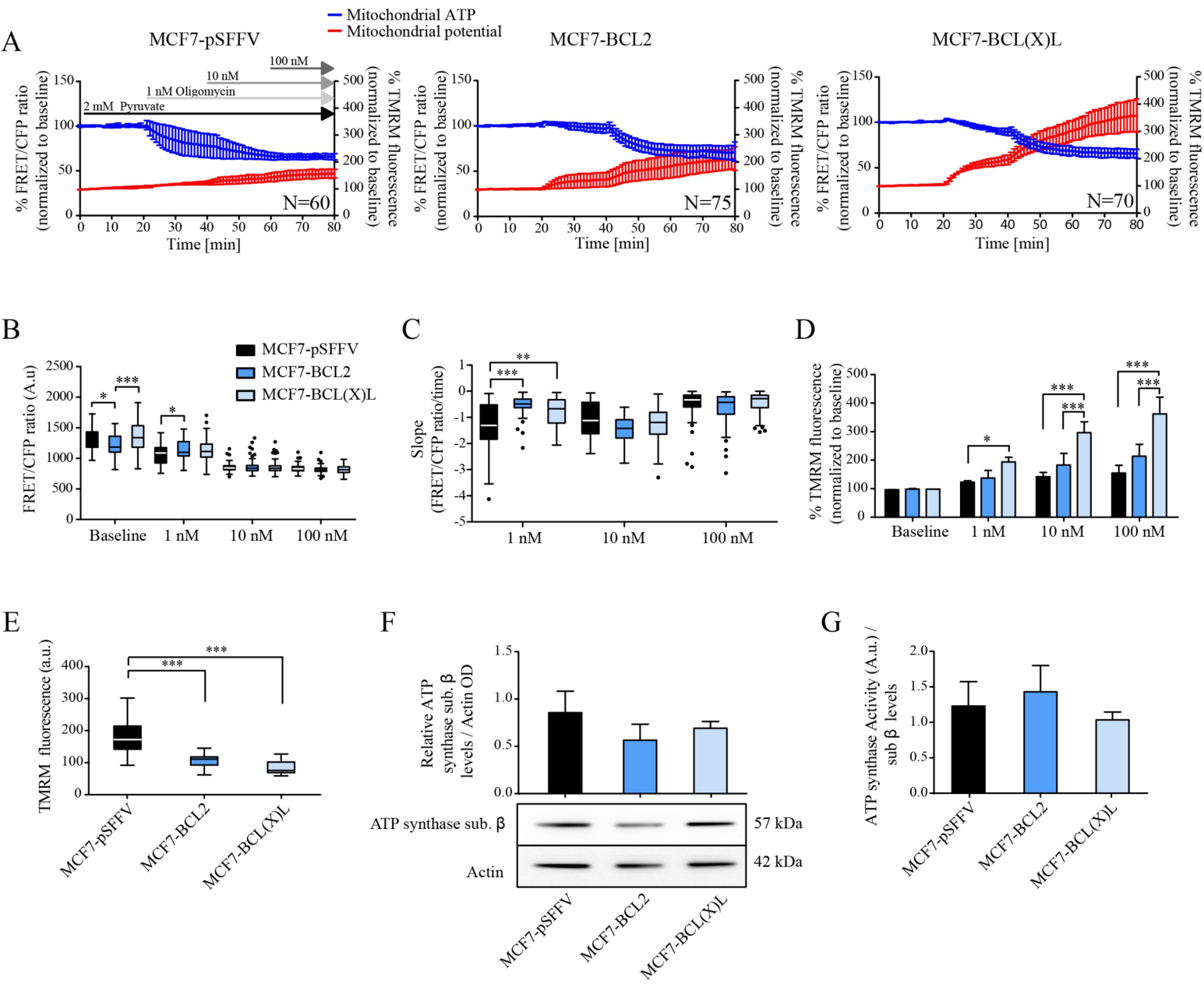


# Figure 4

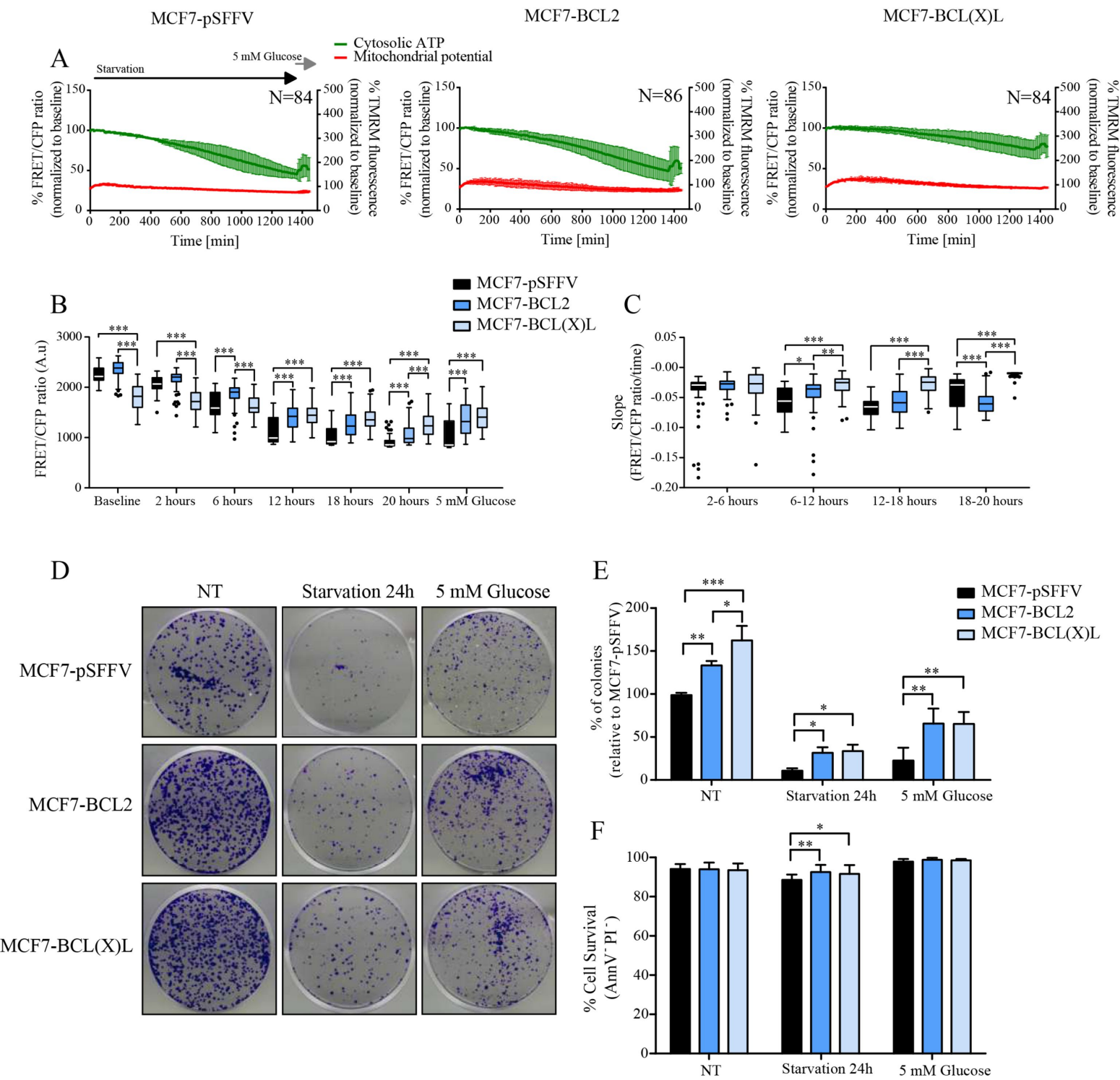


# Figure 5

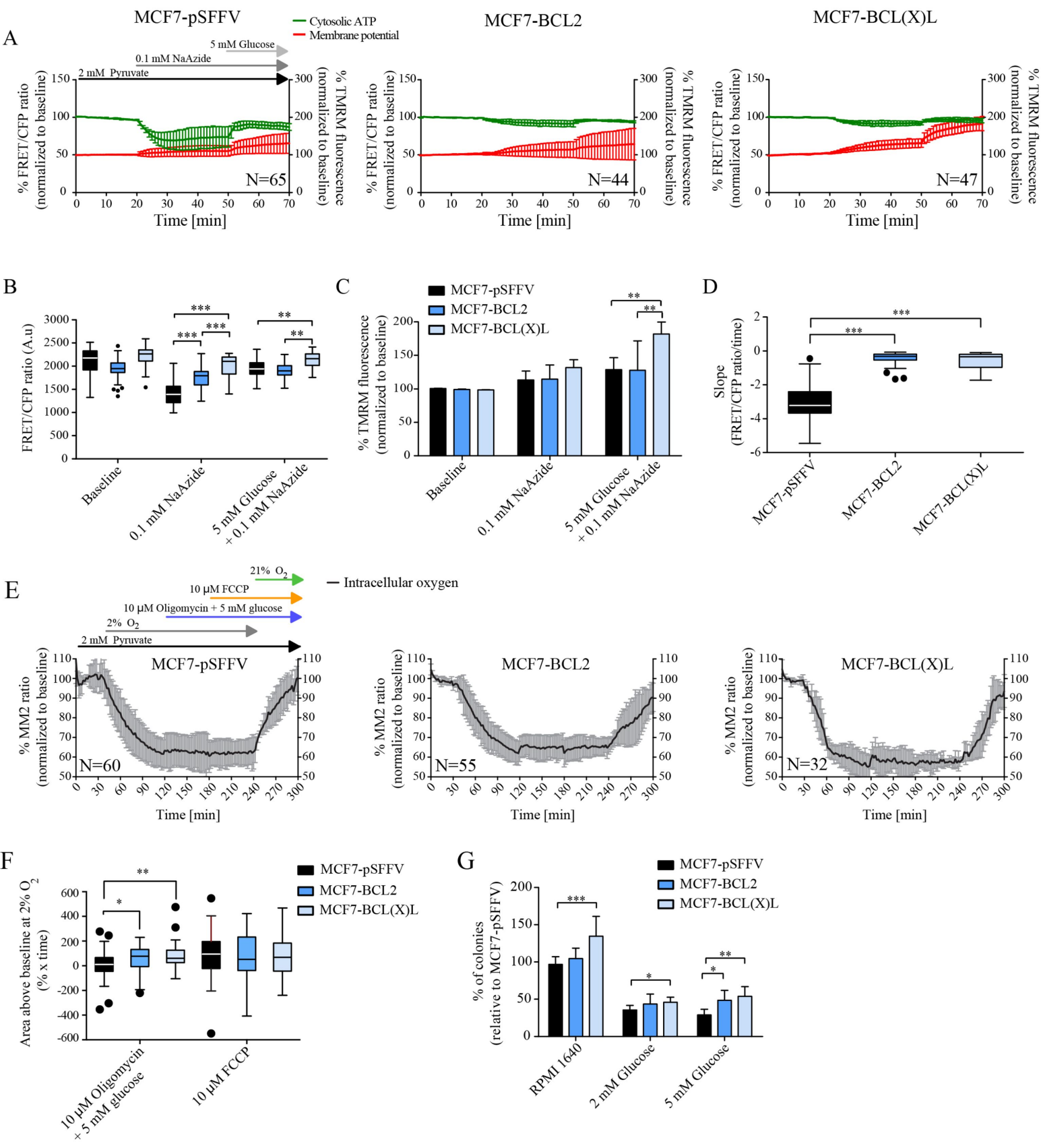


# Figure 6

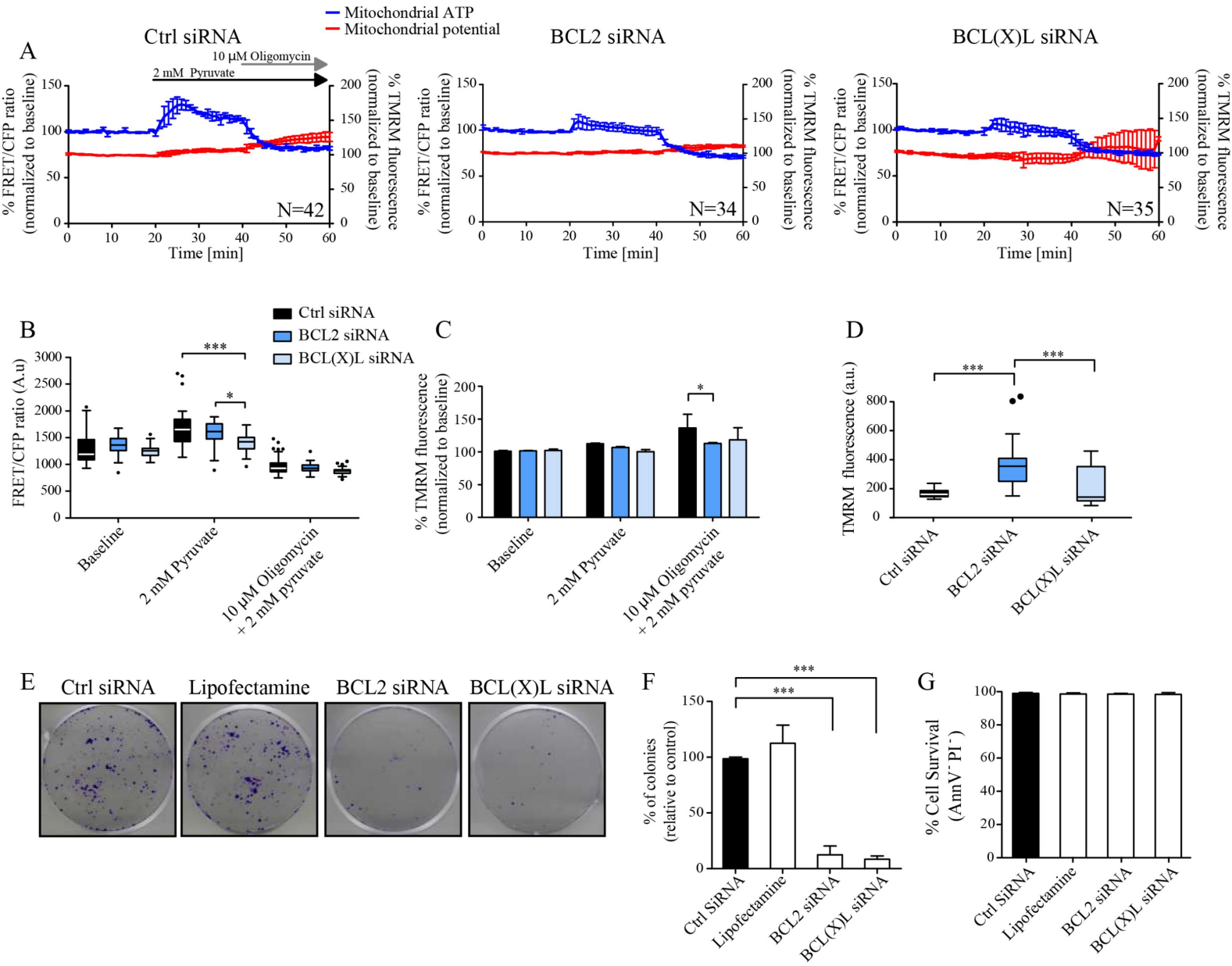


# Figure 7

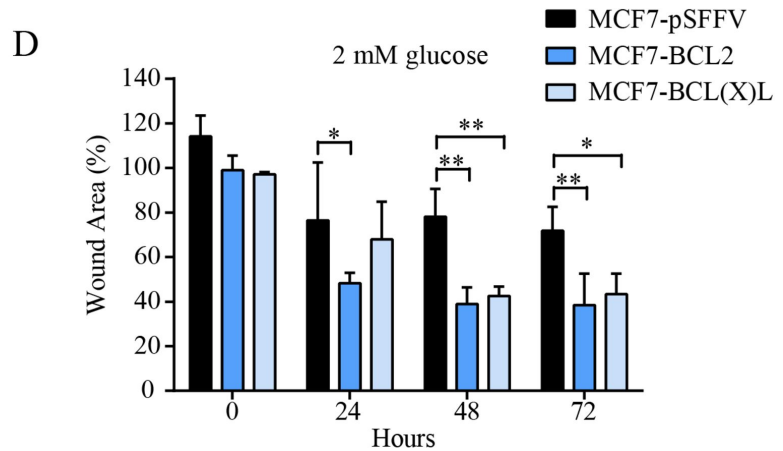
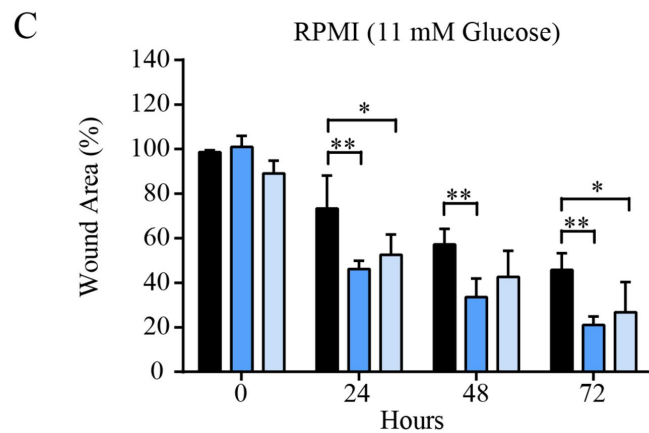
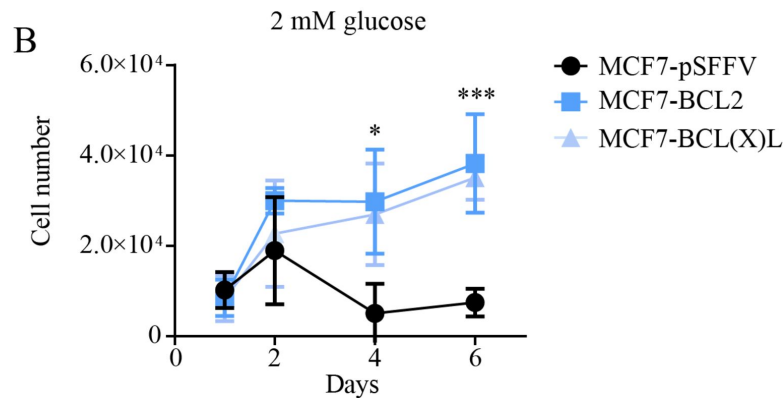
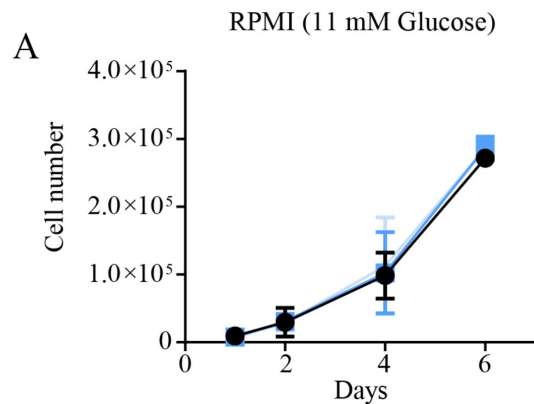




# Figure 8

